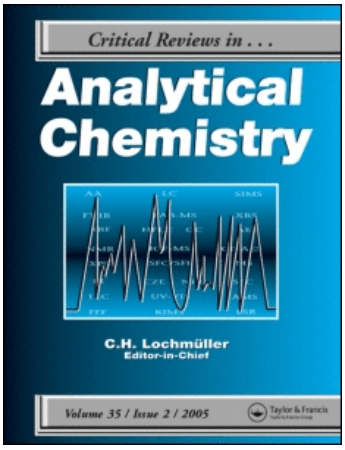

Critical Reviews in Analytical Chemistry
Publication details, including instructions for authors and subscription information:
http://www.informaworld.com/smpp/title~content=t713400837

Fundamental Aspects of Atomic Absorption Spectrometry

Balazs Magyar; L. de Galan

To cite this Article Magyar, Balazs and de Galan, L.(1987) 'Fundamental Aspects of Atomic Absorption Spectrometry', Critical Reviews in Analytical Chemistry, 17: 2, 145 — 191
To link to this Article: DOI: 10.1080/10408348708542793
URL: http://dx.doi.org/10.1080/10408348708542793

FUNDAMENTAL ASPECTS OF ATOMIC ABSORPTION SPECTROMETRY

Author: **Balazs Magyar**
Institute for Inorganic Chemistry
Swiss Federal Institute of Technology
ETH
Zürich, Switzerland

Referee: L. de Galan
Department of Analytical Chemistry
Technische Hogeschool
Delft, Netherlands

I. INTRODUCTION

Modern atomic absorption spectrometry (AAS) only dates back to 1955 to the famous article by Walsh.[1] He showed very clearly for the first time that the absorptivity $k(\lambda_o)$ at the absorption line center λ_o is the quantity that should be measured for analytical purposes.

$$k(\lambda_0) = (8.32 \times 10^{-13}\text{cm}) f_{\ell u} n_\ell \lambda_0^2 / \delta\lambda_a \quad (1)$$

The oscillator strength for the transition from the lower to the upper energy state is $f_{\ell u}$, n_ℓ is the number density of the atoms present in the lower state, and $\delta\lambda_a$ is the half-intensity width of the absorption porfile of the resonance line. As the "measure" $k(\lambda_o)$ is inversely proportional to $\delta\lambda_a$, high sensitivity is obtained for narrow absorption lines.

This idea initiated an enormous activity in the field of AAS. In the course of this rapid development of the methodology of AAS, many important investigations have shown that Equation 1 had to be modified for practical use, especially for estimating sensitivities of determinations by AAS. One of the most important findings of many researchers was that generally a greater number of different species exist in the atom reservoir in question. Alkemade et al.[2] demonstrated this very impressively in their comprehensive book *Metal Vapours in Flames*. As a consequence, the sensitivity S_A of determination of the analyte A by AAS depends also on the fraction atomized β_a ($= [n_a + n_i]/n_t$) and on the degree of ionization γ ($= n_i/[n_a + n_i]$), where n_a and n_i are the number densities of the neutral atoms and ions, respectively, and n_t is the total number density of all species containing the analyte A. The observation that the calibration curves $A(\lambda_o)$ vs. c_A, i.e., absorbance at absorption line center λ_o vs. concentration, are virtually always bent toward the concentration axis was also very important[3] (for an insight into this problem see Reference 4).

In order to comprise the largest possible number of results obtained by many scientists working in the field of AAS into a single equation, the following sensitivity formula was derived:[5-6]

$$S_A = \left[\frac{dA(\lambda_0)}{dc_A}\right]_0 = (2.175 \times 10^5 \text{cm}/\mu\text{mol}) \frac{\beta_a(1-\gamma)\rho}{M_A} \left(\frac{b}{D}\right) \frac{(gf)P_\ell \lambda_0^2}{(\delta\lambda_a^2 + \delta\lambda_s^2)^{1/2}} \quad (2)$$

The original symbols were replaced here by the corresponding IUPAC symbols.

The sensitivity S_A is the initial slope of the calibration curve. The relative atomic mass M_A of the analyte and the density ρ of the solution need no further discussion here. The β_a, γ, weighted oscillator strength (gf), half-intensity width $\delta\lambda_a$, and $\delta\lambda_s$ of the absorption and source line profiles, respectively, and especially the ratio (b/D) of the absorption path length b to the dilution factor D determine the sensitivity of determinations by AAS and will be

discussed in detail. Thereby, Equation 2 will serve as a guideline. $\delta\lambda_a$, β_a, γ, and the population factor P_i have the common feature that they are dependent on the temperature. Therefore, they will be discussed under the heading "Temperature Dependence of the Sensitivity" (see Section II.B).

This equation was obtained for idealized conditions:

1. The monochromator of the atomic absorption spectrometer separates the resonance line λ_o of the analyte atom AI from all other atomic lines, stray radiation, and polychromatic background radiation.
2. Thermodynamic equilibrium is established in the part of the atom reservoir transversed by the radiation of the energy source (mostly a hollow cathode lamp, HCL).
3. The Atomic absorption line profile may be represented by a Gaussian profile near the line center λ_o.

Although these idealized conditions are only roughly approximated in practical work, Equation 2 provided good estimates of the sensitivities of determinations by flame-[5] and ICP-AAS.[6-7] Nevertheless, the importance of the sensitivity formula of Equation 2 consists not in the possibility of making numerical estimates of S_A, but in the concentrated presentation of the most important factors affecting the sensitivity and accuracy of determinations by AAS.

Equation 2 may also be used to "speciation" of interferences:

1. Chemical interferences occur, if $(\beta_a)_a$ and $(\beta_a)_s$ for the analysis "a" and standard "s" solutions are different.
2. Ionization interferences occur if $(\gamma)_a \neq (\gamma)_s$.
3. Physical interferences occur if $(D)_a \neq (D)_s$.

In order to avoid interferences a and b, it is advantageous to realize the optimum conditions $0.99 < \beta_a < 1$ and $\gamma < 0.01$ or the second best choice $(\beta_a)_a/(\beta_a)_s \rightarrow 1$ and $(\gamma)_a/(\gamma)_s \rightarrow 1$ as close as possible. Physical interferences can be avoided by using standard solutions that have the same physical properties as the analysis solutions, i.e., temperature, viscosity, surface tension, etc.

Of course, there are other fundamental aspects of AAS that cannot be discussed on the basis of Equation 2, i.e., selectivity, precision, detection limit, and instrumental influences upon the performance of determinations. These subjects will be discussed in special sections. From the fundamental aspects of methodology and instrumentation, some special applications of graphite furnace AAS, the background correction, and the simultaneous multielement analysis by continuum source AAS will be discussed. In recent years, flames were the atomizers most frequently used in AAS. Nevertheless, a reduced activity in flame AAS may be expected in the near future. Flame AAS will be partly replaced by atomic emission spectrometry (AES) using an inductively coupled plasma (ICP) as atomizer (ICP-AES). On the contrary, ICP-AES cannot supersede the graphite furnace AAS because of the superior sensitivity and selectivity of the latter. High selectivity means in this respect a small probability of mistaking one element for another. This critical review gives reasons for these forecasts.

II. SENSITIVITY, PRECISION, AND ACCURACY OF DETERMINATIONS BY AAS

A. Constructional Influences upon the Sensitivity

1. Graphite Tube Atomizers

The most important factor determining the sensitivity in a first approximation is the ratio

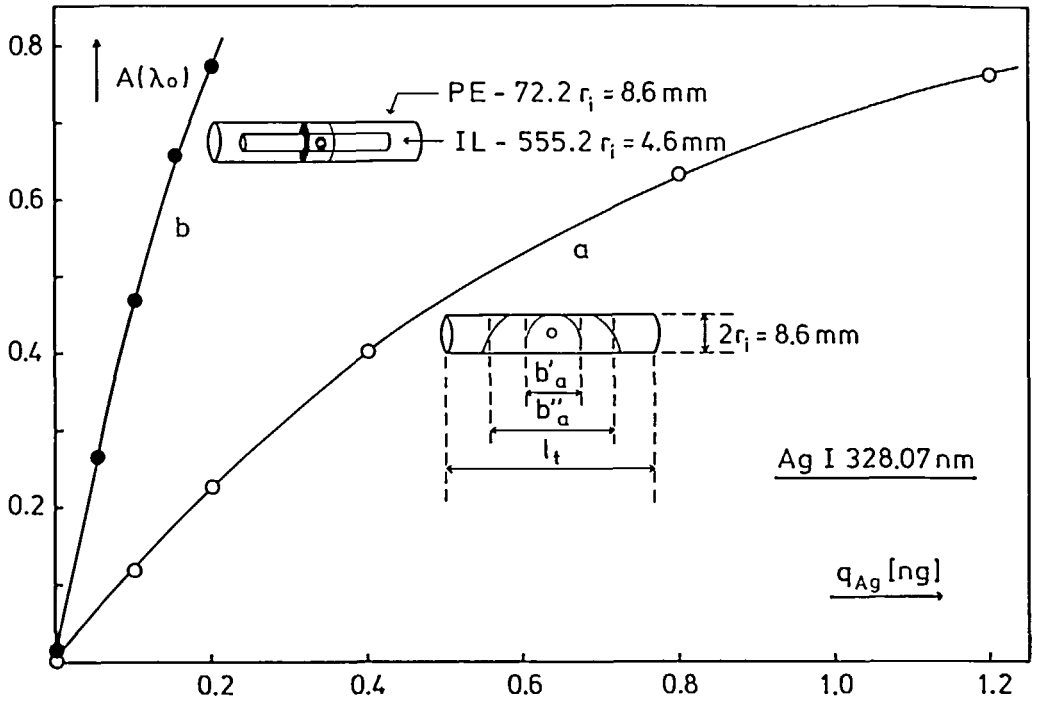

FIGURE 1. Comparison of the calibration curves absorbance $A(\lambda_o)$ vs. quantity q_{Ag} atomized: (a) conventional furnace AAS using a Perkin-Elmer 300 AA-spectrometer and the PE-72 atomizer, (b) tube-in-tube technique[8] using the same AA-spectrometer and the graphite tube of PE-72 as the outer tube and a graphite tube of the Instrumentation Laboratory IL-555 atomizer as the inner tube.

(b/D). The analyst can select the desired sensitivity in a large range by appropriate choice of the atomizer and sample introduction system. This ratio is set in parentheses because it is generally much better known than the separated values of b and D. This may simply be demonstrated in the case of a graphite furnace atomizer. Although the length l_t of the graphite tube is well-known, the absorption path length b is only approximately known because it changes rapidly during the expansion of the atomic cloud in the tube (see momentary lengths b′ and b″ in Figure 1); b is much smaller than l_t at the beginning of the atomization, but it becomes equal to l_t for complete distribution of the analyte atoms in the whole volume of the tube. The dilution factor D is the ratio $(n_t)_s/(n_t)_a$ of the total number densities in the solution "s" and the absorption volume "a". Therefore, in the ideal case of homogeneous distribution of the analyte in the whole volume of the tube and of no analyte losses, D is given by the term bS_t/V_s, where S_t is the cross section of the atomizer tube and V_s the volume of the solution introduced into the tube. As b and D both increase by expansion of the atomic vapor, their ratio (b/D) remains constant as long as the diffusion of atoms out from the tube is small enough to be neglected.

$$(b/D)_{id} = b/(bS_t/V_s) = V_s/r_i^2\pi \qquad (3)$$

It is interesting to note this is the ideal (index "id") case (b/D) and therefore also that the sensitivity S_A is independent of the length of the atomizer tube. Geometrically, S_A is determined by the inner radius r_i of the atomizer tube. If the element in question is determined at the same experimental conditions using the same atomic absorption spectrometer, but two different atomizer tubes of the inner radii $(r_i)_a$ and $(r_i)_b$, respectively, the ratio $(S_A)_b/(S_A)_a$ of

the sensitivities should be proportional to the ratio of the squares of the radii. This may be easily shown by combining Equations 2 and 3:

$$(S_A)_b/(S_A)_a = (r_i^2)_a/(r_i^2)_b \quad (4)$$

This enhancement of sensitivity should also be obtained for the tube-in-tube technique.[8] For the illustration of this technique, a calibration curve was first determined with the usual single-tube technique using a Perkin-Elmer PE-300 atomic absorption spectrometer (see curve a in Figure 1). Thereafter a smaller Instrumentation-Laboratory IL-555 tube was installed into the large PE-72 tube, and the calibration curve b was determined. The ratio $(S_{Ag})_b/(S_{Ag})_a$ of the sensitivities obtained by parabolic regression amounted to 4.5. This value is markedly higher than 3.5 calculated from Equation 4 using the diameters given in Figure 1. Obviously, the geometrical effect upon the number density of the analyte is enhanced by secondary effects, like the absence of recombination of atoms to clusters or/and refractories, because the atomization occurs in an environment of higher temperature. Although the measured values[9] or $(S_A)_b/(S_A)_a$ agree quite well with their predictions from Equation 4 using $(b/D)_{id}$ values from Equation 3, the theoretical values $(S_A)_{id}$ from Equation 2 deviate strongly from the experimental values $(S_A)_{ex}$. For example, 100 $(S_A)_{ex}/(S_A)_{id}$ was only 10, 33, and 6% on average for A = Ag, Cd, and Cr, respectively. Thereby, the average values were determined and calculated for the two graphite tubes shown in Figure 1 and for the tube-in-tube setup. The fact that $(S_A)_{ex} \ll (S_A)_{th}$ is due to the beginning of the diffusion of the analyte from the graphite tube just after the beginning of atomization. Therefore, the maximal number density $(n_a)_p$ at peak-absorbance is determined by kinetics of atomization and degradation of the atomic cloud.

These phenomena were first studied in detail by L'vov,[10] the pioneer of the "graphite cuvette" technique of AAS. In his treatment the number N_p of atoms present at the peak absorbance A_p is given by

$$N_p/N_o = (t_r/t_a)[1 - \exp(-t_a/t_r)] \quad (5)$$

where N_o is the number of analyte atoms injected into the graphite tube having the length l_t and cross section S_t, t_a, the atomization time, and t_r, the main residence time of the analyte atoms in the observation volume V_{eff}. Because of the uncertainty involved in V_{eff}, $(n_a)_p = N_p/V_{eff}$ cannot be calculated accurately. Nevertheless, the ratio $(n_a)_p/(n_a)_o$, and therefore, the ratio A_p/A_o of the corresponding absorbances are given by N_p/N_o to a good approximation. If $t_a/t_r \ll 1$, then $[1 - \exp(-t_a/t_r] \simeq t_a/t_r$, which has the consequence that $N_p/N_o \simeq 1$, peak-absorbance A_p becomes a measure of the number N_o of atoms in the sample injected. Considering only the diffusion through the ends of the graphite tube and neglecting analyte losses by diffusion through the sample introduction hole and by possible diffusion through the porous walls of the tube, the mean residence time is given by[10]

$$t_r = l_t^2/8D = l_t^2/8D_o(T/T_o)^n(P_o/P) \quad (6)$$

where D and D_o are the diffusion coefficients of the analyte atoms at the tube temperature T, and at standard temperature (T_o = 298 K), and pressure (1 atm = 0.1 MPa). The main residence time t_r can be enhanced by the use of long tubes and by working at enhanced pressure P. The power n of the relative temperature T/T_o is obtained from measurements of the diffusion coefficient D at different temperatures[10] (n = 1.6 was obtained in the temperature range of 1100 to 2600 K).

The final results of the treatment by L'vov may be summarized in the following expressions:[10]

$$A_p = K_p(T^{0.7}/P)q_A/S_t \quad (7)$$

$$\int A(t)dt = K_i(l_t^2/T^{0.9})q_A/S_t \quad (8)$$

At a glance of these expressions, it becomes evident that both measures the peak-absorbance A_p and also the integrated absorbance $\int A(t)dt$ increased with decreasing cross section of the tube. A_p and $\int A(t)dt$ bear about the same relationship of opposite sign to the temperature. When integrated absorption is measured, the effects of pressure are eliminated, but the length of the tube becomes of great importance. The proportionality constants K_p und K_i must be determined by measurement of A_p and $\int A(t)dt$, respectively, for known amounts q_A of the analyte injected into the tube.

According to the basic expression Equation 5, there are two possibilities to enhance the peak-absorbance A_p ($\propto N_p$): (1) reduction of the time t_a of atomization and (2) prolongation of the main residence time t_r in the atomizer. Procedures for the reduction of t_a consist in (1) thermal flashing of a good conductor, e.g., a graphite filament[11] used as support for the sample; (2) use of probe techniques, e.g., use of very lightweight graphite support[12] for the sample or a fast wire introduction system;[13] and (3) imposing a very high heating rate that can be realized by discharging a bank of capacitors across the graphite furnace.[14-15]

The prolongation of the main residence time t_r by lengthening the atomizer would be very effective because t_r increases with the square of the tube length l_t (see Equation 6). However, it is difficult to construct long-tube atomizers that can be heated rapidly, thus the gain in N_p/N_o, due to prolongation of t_r, is lost by increase of t_a (see Equation 5). An alternate way to increase t_r consists in restriction of the total area of the orifices through which the analyte vapor escapes.[10] Adding cups and/or plugs to commercially available atomizers (CRA) increased the atomic residence time and hence peak height as well as peak absorbances.[16] The increase of t_r and the heating rate of the furnace determine the effective gas phase temperature T_{eff}. The increase in T_{eff} is most important because it usually leads to a lessening of the gas-related matrix effects. In practical analytical work, at least four processes[13] must be considered as being responsible for the loss of atomic vapor from a heated graphite furnace: (1) diffusion of atoms through the apertures and porous walls of the furnace, (2) convection, (3) expulsion by sample vapor, and (4) the interaction of free atoms with the furnace wall. Therefore, the residence time t_r depends not only on the atomizer used but also on the chemical properties of the analyte and on the quantity of accompanying substances. Relative volatile elements, such as Ag, Cd, Zn, and Pb, which do not form compounds with graphite, are expected to disappear by a diffusion-controlled mechanism. On the contrary, dissipation of elements, such as Cu, Fe, Ni, Mn, and especially of those forming stable carbides or intercalation compounds with graphite appears to be governed by the redeposition process.[17]

The atomization time t_a depends also on many factors, among them the heating rate α ($= dT/dt$) and the activation energy E_a are the most important, presumably. According to the kinetic model proposed by Torsi and Tessari,[18] the rate of the release of analyte from the surface is proportional each time to the number of analyte atoms still retained on the surface. Furthermore, the variation of the kinetic constant of the release of the atoms with the atomizer heating can be accounted for by an Arrhenius type expression, which involves the introduction of the activation energy E_a for the rate determining step. Following this fundamental idea, a number of attempts were undertaken in order to describe relationships between heating rate and peak height in electrothermal AAS. The discussion of these kinetic theories is beyond the scope of this review (for an insight see Reference 19). Only one relationship derived from Zhou et al.[20] will be discussed here.

$$N_p/N_o = (k_p/k_R)\exp[-(T_p - T_o)k_m T_m^2/\alpha T_p T_o] \quad (9)$$

k_p and k_R are the rate constants [s^{-1}] of the atom formation and dissipation at the peak absorbance A_p. T_o is the tube temperature [K] corresponding to first appearance of the atomic absorption signal, T_p, the tube temperature at peak absorbance and α, the linear heating rate [Ks^{-1}]. k_m is the constant of atom formation at temperature T_m, where $T_o < T_m < T_p$. For the most analytical conditions, T_m^2 is approximately equal to $T_p T_o$, which results

$$N_p/N_o = (k_p/k_R)\exp[-(T_p - T_o)k_p/\alpha] \quad (10)$$

at peak absorbance. The rate constant of atom formation k_p at peak absorbance is given by[18,20]

$$k_p = E_a\alpha/RT_p^2 \quad (11)$$

where R is the universal gas constant. Introduction of this term into Equation 10 results in a relationship which clearly shows that N_p/N_o, and therefore the peak height should increase linearly with increasing heating rate.

In order to obtain a constructional factor $(b/D)_t$ for real tube conditions, the ideal term from Equation 3 should be multiplied by N_p/N_o from Equations 5 or 10, e.g.:

$$(b/D)_t = (V_s/r_i^2\pi)[(t_r/t_a)(1 - \exp(-t_a/t_r))] \quad (12)$$

Unfortunately, the calculation of sensitivities from Equation 2 using this constructional factor is hindered by the fact that t_a and t_r are generally not known. Perhaps the reverse procedure could have more importance for spectrochemical characterization of the elements. The ratio of sensitivities is determined by measurement of $(S_A)_{ex}$ and calculation of $(S_A)_{id}$ using the constructional factor$(b/D)_{id}$, and then t_a/t_r is calculated from the following relationship:

$$(S_A)_{ex}/(S_A)_{id} = (t_r/t_a)[1 - \exp(-t_a/t_r)] \quad (13)$$

For a given sensitivity ratio, the corresponding time ratio t_a/t_r is easily obtained from a plot of the values of the right side term of this equation vs. the corresponding preselected values of t_a/t_r. From the sensitivity ratios 0.33, 0.10, and 0.06 given above for A = Cd, Ag, and Cr, respectively, the time ratios t_a/t_r of 2.9, 10, and 17 were obtained. Apparently, the increasing order of t_a/t_r is reversed to the order of increasing volatility of the metals. This finding suggests that t_a is small for volatile metals and at the same time it is less dependent on the kind of the metal in question so far as no chemical reactions with the graphite occur.

2. Flames and ICP

The dilution factor D for flames and ICP can be calculated from the volume flow rates F and the efficiency of nebulization ϵ_n. The ratio of the amount of analyte entering the flame or ICP to the amount of analyte aspirated is ϵ_n. It can easily be estimated by weighing the liquids (solutions) corresponding to $t \cdot F_\ell$ and $t \cdot F_b$ mℓ, where t is the time needed for the accumulation of ca. 20 mℓ back flow $t \cdot F_b$: $\epsilon_n = (F_\ell - F_b)/F_\ell$. Assuming that the flame or ICP may be considered as a mixture of ideal gases, one obtains from the equation of state modified for steady state systems[6,7] (see Figure 2).

$$D = (F_\ell\epsilon_n)^{-1}[(F_u(\nu_a/\nu_o) + \nu_s\rho F_\ell\epsilon_n RT_o/M_sP](T_a/T_o) \quad (14)$$

ν_s is the number of species originating from the dissociation of the solvent molecule (e.g., three in ICP in the case of H_2O), R, the universal gas constant, M_s, the relative mole mass of the solvent, and P is the atmospheric pressure. T_a and T_o refer to the temperature of the gases in the atomizer and room temperature, respectively. ν_a/ν_o is the ratio of the total number of moles of the products per unit volume of the atomizer to the total number of moles per unit volume of the gas mixture at room temperature. Although the ratio ν_p/ν_e of moles of products and educts is smaller than one in the case of the air/acetylene flame, ν_a/ν_o becomes greater than one because of the partial dissociation of the products of the stoicheiometric reaction.[21]

$$C_2H_2 + 5/2\ O_2 + 10\ N_2 = 2\ CO_2 + H_2O + 10\ N_2$$

$$\nu_p/\nu_e = 0.963 \quad (15)$$

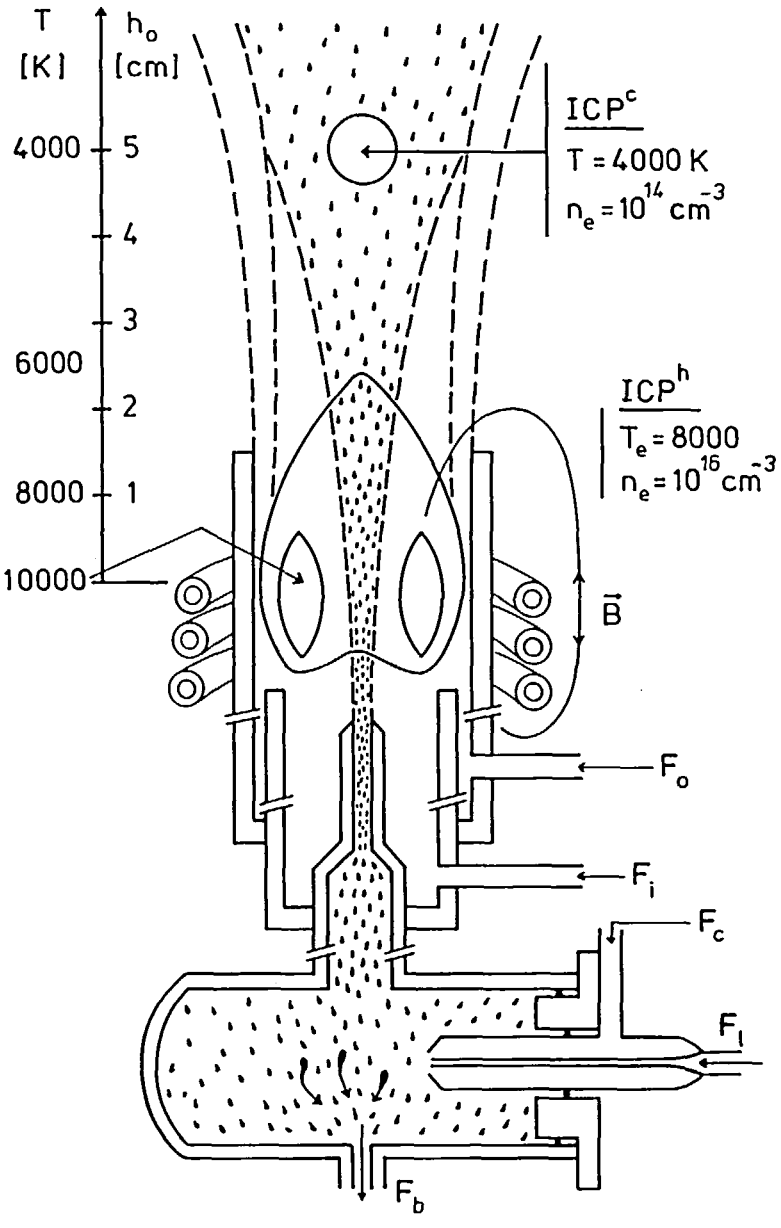

FIGURE 2. A three-tube configuration of a demountable plasma torch (joint rings are omitted for simplicity). The solution is taken up with a volume flow rate F_ℓ generally provided with a peristaltic pump. The small droplets, produced by the concentric glass capillary nebulizer, are transported by the carrier gas having the volume flow rate F_c into the plasma. In the case of water as solvent, about 99% of the solution aspirated appears in the form of large droplets that separate out from the aerosol giving the back flow F_b. The intermediate gas and the outer gas flow through the intermediate tube and the outer tube with the volume flow rates of F_i and F_o, respectively. The magnetic flux density $\vec{B}$, shown around the water cooled copper coils, changes its direction with a high frequency, mostly 27 MHz. The temperature and number density n_e of electrons decrease with increasing observation height h_o above the coil. ICP-AAS and ICP-AES measurements are carried out in the "cold zone" ICP^c and the "hot zone" ICP^h, respectively.

Table 1
THE MOST IMPORTANT CHARACTERISTICS OF THE ATOMIZERS USED IN THIS WORK

Atomizer	T_a,[K]	n_e,[cm^{-3}]	ν_a/ν_o	M_C,[g/mol]	(b/D),[cm] PE	(b/D),[cm] IL
Graphite tube furnace	1500 to 3000	3×10^{11}	1.0	40(Ar) or 28(N_2)	1.8×10^{-2}	6.3×10^{-2}
Air/C_2H_2	2500	4×10^{10}	1.03	30	—	3.3×10^{-5}
N_2O/C_2H_2	3000	6×10^{10}	1.64	31	—	5.0×10^{-6}
ICP	~4000	$\sim 10^{14}$	1.0	40	1.3×10^{-6}	—

Note: T_a = gas kinetic temperature in the atomizer, n_e = number density of free electrons, (ν_a/ν_o) = ratio of the mol numbers at atomizer and room temperature (T_a and T_o), respectively, M_C = relative mol mass for collision half-intensity width calculations, and (b/D) = the ratio of the absorption path length and the dilution factor; atomic absorption spectrometer used: Perkin-Elmer PE-300 with HGA-72 atomizer, and Instrumentation Laboratory IL-751 with CTF-555 atomizer, and PE-300 optically coupled to ICP of Radyne-50 RF-generator (at 1.3 kW into the ICP and 5 cm observation height); (b/D) ratios are typical but not fixed throughly.

$$C_2H_2 + 5\ N_2O = 2\ CO_2 + H_2O + 5\ N_2$$

$$\nu_p/\nu_e = 1.333 \tag{16}$$

Usually, the flames are operated under such oxidant flow rates that combustion yields CO rather than CO_2. In that case ν_p/ν_e enhances to 1.059 and 1.500, respectively, which are in better agreement with the "real" values (see Table 1).

The second term in brackets of Equation 14 adds only a few percent to the volume flow rate F_u of the unburnt mixture and will be omitted in the further discussion. The volume flow rate of unburnt gas mixture is given by the sum of the volume flow rates of the fuel and oxidant resulting in the following equation for the dilution factor D_f of flames (index "f"):

$$D_f = (F_\ell \epsilon_n)^{-1}[(F_{fu} + F_{ox})(T_a/T_o)(\nu_a/\nu_o)] \tag{17}$$

The estimation of the volume flow rate F_m of the plasma gas mixture for the three-tube configuration of a plasma torch is more difficult, because the mixing of the carrier gas (or aerosol gas F_c) and the intermediate gas (F_i) occurs not suddenly but continuously with increasing height agove the coil (whereas F_i is small or even 0 in ICP-AES, $F_i > F_c$ in ICP-AAS using the ICP shown in Figure 2). Nevertheless, it may be assumed that the two gases are almost completely mixed together at an observation height h_o of 5 cm, but only a small mixing with the coolant (outergas, F_o) occurs at this height. Only this "cold" zone of ICP is suitable for ICP-AAS, because the atomic emission intensity of the analyte in the hot zone of ICP approaches the intensity of the source hollow cathode lampe (HCL) and no atomic absorption measurements can be made.[7] Furthermore, an observation height of 3 to 5 cm is more suitable for ICP-AAS because of the reduced radiance of the ICP at heights above ca. 3 cm;

$$D_p = (F_\ell \epsilon_n)^{-1}[(F_c + F_i)(T_a/T_o)] \tag{18}$$

b/D values with other important characteristics of atomizers are compiled in Table 1. The

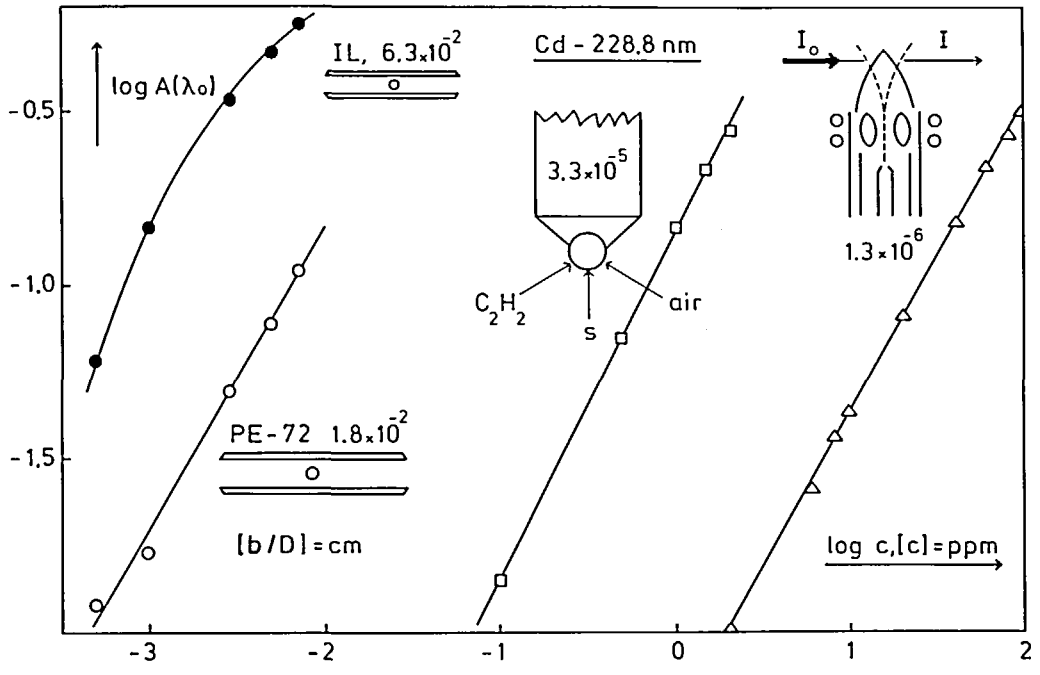

FIGURE 3. Dependence of the working range of the calibration curves upon the ratio b/D whereby b is the absorption path length and D the dilution factor. The calibration curves absorbance $A(\lambda_o)$ vs. concentration c are shown as double logarithmic plots because of the large concentration range covered by the methods furnace AAS, flame AAS, and ICP-AAS.

absorption path length was approximated by the slit length of the burner and the diameter of the intermediate tube in the case of flames and ICP, respectively. Construction factors b/D for the hydride generation technique and for the mercury cold vapor method were not included in this table because the corresponding values are quite different from one setup to the other. The dilution factor D is simply given by the volume ratio V_g/V_s, where V_g is the volume of the gas phase containing Hg or the hydride MH_n with M = As, Bi, Ge, Sn, Te, and n = 2, 3, or 4 and V_s, the volume of the solution taken for the generation of Hg(g) or $MH_n(g)$, respectively. The most favorable construction factors up to 10 cm can be realized for this technique resulting in the highest sensitivities of determinations by AAS.

The sensitivities S_A, and as a consequence, the lower limit of the working ranges of calibration curves are determined by (b/D) in a first approximation. In order to demonstrate this conclusion drawn from Equation 2, calibration curves $A(\lambda_o)$ vs. c_{Cd} for the Cd determinations at the Cd I 288,8 nm resonance line were determined using four different atomizers (see Figure 3). The smallest construction factor (b/D) and the lowest sensitivity were obtained for ICP transversed radial by the light of the HCL. This is a consequence of the reduced path length b. The largest b/D value and therefore the highest sensitivity was realized with the small graphite tube having an inner radius r_i of 2,3 mm. In order to work in the quasi-linear range, more diluted solutions should be measured using the small atomizer. For simplicity, portions of the same standard solutions were injected into both graphite tubes.

B. Temperature Dependence of the Sensitivity

Although the temperature T_a of the atomizer does not appear in Equation 2, it determines the fraction atomized β_a, the degree γ of ionization, the population of the lower energy state of the analyte atom P_ℓ, and the half-intensity width $\delta\lambda_a$ of the absorption profile of the resonance line λ_o in question. T_a also appears in terms for the construction factor (b/D).

The temperature dependence of the sensitivity is discussed in the next sections. In order to facilitate the discussion on the importance of these factors for the sensitivity of determinations by AAS, the elements will be classified according to their thermochemical behavior:

1. Elements, which form little or no stable compounds and do not ionize significantly in flames and graphite furnace atomizers up to ca. 3000 K. The first ionization energy[22] of these elements is high and the bond dissociation energy[2,21] of their monoxides AO is small. Generally, these elements are easily determined in all four atomizers cited in Table 1 as the ideal conditions $\beta_a \rightarrow 1$ and $\gamma \rightarrow 0$ can be realized in a wide range of temperatures T_a and number densities n_e of free electrons, e.g., Cd, Hg, Zn, etc.
2. Elements, which form no refractory compounds ($\beta_a \rightarrow 1$), but have low first ionization energy. The air/C_2H_2-flame is to be preferred for the determination of these elements because of the smaller degree of ionization resulting in a higher sensitivity and in lower operation costs, e.g., Na, K, etc.
3. Elements, which form refractory compounds and have high until relatively low ionization energy, e.g., Al, Si, etc. The ICP is the most suitable atomizer because of its high temperature T_a and number density n_e of free electrons, which results in ideal conditions: $\beta_a \rightarrow 1$ and γ = constant. Nevertheless, the N_2O/C_2H_2-flame buffered on free electrons give a higher sensitivity than ICP-AAS because of the more favorable ratio (b/D) (see Table 1). Of course, ICP-AES makes more sensitive determinations possible than ICP-AAS and AAS using the N_2O/C_2H_2-flame.

It should be stressed, that elements of all three classes can be determined by AAS using a graphite furnace atomizer at appropriate experimental conditions including surface modification, e.g., covering the graphite surface by W or Ta carbide in order to prevent analyte losses by carbide formation. For the discussion of the temperature dependence of the sensitivity, 32 elements were selected. Their most important spectrochemical characteristics are given in Table 2.

1. The Spectroscopic and the Population Factor

The population factor P_ℓ of the lower energy state "ℓ" of the atom (or ion A II) decreases with increasing temperature T (= T_a) as the partition function Z_A increases with T:

$$P_\ell = [Z_A(T)]^{-1}\exp[-(E_\ell - E_0)/kT] \quad (19)$$

$$Z_A(T) = \Sigma_0^{m^*}(2J_m + 1)\exp[-(E_m - E_0)/kT] \quad (20)$$

E_ℓ and E_O are the energy levels of the lower and ground state of the analyte, respectively, k the Boltzmann constant, and J the angular quantum number of the energy state in question. m is the running number of energy states including 0, 1, . . . , ℓ, . . . , u, . . . , m*. $Z_A(T)$ and P_ℓ can be calculated with any desired accuracy if the energy levels E_m of the analyte are completely known. Since this is usually not the case, the cutoff criteria, i.e., the choice of the limiting term T_{m^*} influences $Z_A(T)$[23] and therefore P_ℓ.[7]

The temperature dependence of the population factor P_ℓ is mainly governed by $Z_A(T)$ because ($E_\ell - E_0$) is 0 or much smaller than kT (see legend to Table 2). For further discussions, the values obtained from polynominal expressions will be used, whereby the values will be rounded off to 0.01, which is the inaccuracy of the curve fitting procedure used for the calculation of the polynominal expressions.[24]

For reasons of simplicity, we will combine the spectroscopic characteristics of the resonance line λ_o to a spectroscopic factor Λ:

$$\Lambda = 2(\ln 2/\pi)^{1/2}(gf)\lambda_o/(\delta\lambda_a^2 + \delta\lambda_s^2)^{1/2} \quad (21)$$

$$\delta\lambda_a = [\delta\lambda_D^2 + \delta\lambda_C^2]^{1/2} \text{ at } T = T_a \quad \text{and} \quad \delta\lambda_s = \delta\lambda_D \text{ at } T = T_s \quad (22)$$

Table 2
SPECTROCHEMICAL CHARACTERISTICS OF THE ELEMENTS SELECTED FOR THE DISCUSSION OF THE SENSITIVITY OF DETERMINATIONS

Analyte/ class	λ [nm]	(gf) [1]	Lower-upper term	E_i[22a] [eV]	D_o [eV]
Ag / a	328.07	0.90 B	$^2S_{1/2} - {}^2P^o_{3/2}$	7.576	2.0
Al / c	309.27	0.64 C	$^2P^o_{3/2} - {}^2D_{5/2}$	5.986	5.0
As / c	193.70	0.45 D	$^4S^o_{3/2} - {}^2P_{3/2}$	9.81	4.9
Au / a	242.80	0.53 D	$^2S_{1/2} - {}^2P^o_{3/2}$	9.225	—
B / c	249.68	0.16 C	$^2P^o_{1/2} - {}^2S_{1/2}$	8.296	8.2
Ba / c	553.55	1.59 C	$^1S_o - {}^1P^o_1$	5.212	5.7
Ba^+ / c	455.40	1.46 A	$^2S_{1/2} - {}^2P^o_{3/2}$	10.004	—
Ca / c	422.67	1.75 B	$^1S_o - {}^1P^o_1$	6.113	4.3
Ca^+ / c	393.37	1.36 C	$^2S_{1/2} - {}^2P^o_{3/2}$	11.871	—
Cd / a	228.80	1.25 C	$^1S_o - {}^1P^o_1$	8.993	<3.8
Cr / c	357.87	2.56 B	$^7S_3 - {}^7P^o_4$	6.766	4.5
Cu / a	324.75	0.88 B	$^2S_{1/2} - {}^2P^o_{3/2}$	7.726	4.1
Eu / c	459.40	4.43 D	$^8S^o_{7/2} - {}^8P_{9/2}$	5.67	5.8*
Fe / a	248.33	5.00 C	$^5D_4 - {}^5F^o_5$	7.87	4.2
Hg / a	253.65	0.038 D	$^1S_o - {}^3P^o_1$	10.437	—
In / b	303.94	0.72 D	$^2P^o_{1/2} - {}^2D_{3/2}$	5.786	3.5
K / b	766.49	1.36 B	$^2S_{1/2} - {}^2P^o_{3/2}$	4.341	3.5
Mg / a	285.21	1.81 B	$^1S_o - {}^1P^o_1$	7.646	4.0
Mn / a	279.48	3.47 C	$^6S_{5/2} - {}^6P^o_{7/2}$	7.435	4.1
Mo / c	313.26	1.4	$^7S_3 - {}^7P^o_4$	7.099	5.0
Na / b	589.00	1.30 A	$^2S_{1/2} - {}^2P^o_{3/2}$	5.139	3.3
Ni / a	232.00	6.12 C	$^3F_4 - {}^3G^o_5$	7.635	4.0
Pb / a	283.31	0.21 D	$^3P_o - {}^3P^o_1$	7.416	3.9
Pd / a	247.64	0.1	$^1S_o - {}^3D^o_1$	8.34	2.4*
Pt / a	265.95	0.87	$^3D_3 - {}^3F^o_4$	9.0	3.5*
Rb / b	780.02	1.35 B	$^2S_{1/2} - {}^2P^o_{3/2}$	4.177	3.7
Se / c	196.03	0.59	$^3P_2 - {}^3S^o_1$	9.752	4.3
Si / c	251.61	0.57 C	$^3P_2 - {}^3P^o_2$	8.151	8.2
Sn / c	224.61	0.363 D	$^3P_o - {}^3D^o_1$	7.344	5.5
Sr / b	460.73	1.92 B	$^1S_o - {}^1P^o_1$	5.695	4.2
Sr^+ / b	407.77	1.42 C	$^2S_{1/2} - {}^2P^o_{3/2}$	11.030	—
Ti / c	365.35	1.45 C	$^3F_4 - {}^3G^o_5$	6.82	7.2
Tl / b	276.79	0.58 C	$^2P^o_{1/2} - {}^2D_{3/2}$	6.106	—
Zn / a	213.86	1.46 B	$^1S_o - {}^1P^o_1$	9.394	2.8

Note: λ = wavelength, (gf) = weighted oscillator strength[22,44] terms involved in the transition, E_i = first ionization energy of the analyte (E_i of the ion A^+ = second E_i of the atom A), and bond dissociation energy D_o of the monoxides AO and those of the hydroxides in the case of alkali metals (class b). The weighted oscillator strengths were calculated from transition probabilities given in Reference 22. The estimated uncertainties of (gf) are indicated by code letters as follows: A-uncertainties within 3%, B- within 10%, C- within 25%, and D- within 50%. D_o values were selected from the compilations of References 2, 21. Values marked with a star are strengths of chemical bonds[22c] recalculated from kJ/mol into eV. The classification of the analytes into classes: (a) $E_i \geq 7.0$ and $D_o \leq 4.2$, (b) $E_i \leq 7.0$ and $D_o \leq 4.2$, (c) the rest of analytes. The lower term is the ground term for all transitions except the transitions of Al, Si, and Ti for which the energy difference ($E_1 - E_o$) amounts to 112, 223, and 387 cm^{-1}, respectively.

The half-intensity widths $\delta\lambda_D$ for pure Doppler broadening were calculated by assuming that the temperature of the analyte in the source (in the hollow cathode) T_s and in the atomizer T_a are identical with the corresponding gas kinetic temperatures T.

$$\delta\lambda_D = 7.162 \times 10^{-7}\,\lambda_o(T/M_A)^{1/2} \tag{23}$$

The collision or "pressure" broadening of the resonance line λ_o arising from the transition "0 ⇆ u" is given by

$$\delta\lambda_C = (1.76 \times 10^{16} g^{1/2}K^{1/2}/Pa \cdot m^3 mol^{1/2})P_C(\sigma_C/\pi)\lambda_o^2\left[\left(\frac{1}{M_A} + \frac{1}{M_C}\right)/T\right]^{1/2} \tag{24}$$

For lines with $(E_\ell - E_O) > 0$ (see, e.g., Al, Si, and Ti in Table 2) the half-intensity width for pure collision broadening is given by $2\delta\lambda_C$ as the collision probabilities of both unstable states "u" and "ℓ" must be taken into account.

The collision cross section of the analyte A with respect to the colliding particle C is σ_C. In Equation 24 (σ_C/π) is introduced in the place of σ_C. Therefore, the numerical factor was enlarged by π. The reason is that in most literature reports on flame experiments the value of (σ_C/π) instead of σ_C is communicated.[2] As the collision cross sections for a great number of the 35 analyte species of Table 2 were not available in the literature, the same collision cross section σ_C/π of 6×10^{-19} m^2 was used for all analyte perturber combinations. The collisions of the excited analyte atoms with neutral atoms and molecules also cause a line shift,[2] generally toward longer wavelengths. The ratio of this shift to the half-intensity width is: $\Delta\lambda_C/\delta\lambda_C = 0.36$. This theoretical value is not well-proved by experiments up to now. Therefore, we will not discuss the influence of line shifts upon the sensitivity in detail. The collisions of A with ions and electrons (Ar^+ and e^-) in ICP cause an additional Stark broadening, $\delta\lambda_S$, and a shift of the absorption line. With exception of hot plasmas (T > ca. 6000 K) $\delta\lambda_S$ is much smaller than $\delta\lambda_C$ and will be neglected also.

The calculation of $\delta\lambda_a$ from Equation 22 is not quite correct as the addition of "variances" is only justified for pure Gaussian profiles. Collision and Doppler broadening act independently and lead to a Gaussian and Lorentzian profile, respectively. The resulting profile is a Voigt profile.

Although the use of Voigt profiles is almost self-evident in basic research of atomic spectroscopy, its use is very limited in analytical atomic spectrometry until today for the following reasons:

1. The quality of estimations of sensitivities is not limited by the choice of the line profile model but by the uncertainties of other factors, especially (gf), (b/D), and β_a. Therefore, a simpler model may be preferred.
2. The use of Voigt profiles would be straightforward if accurate line broadening a-parameters would be available. In fact, only a very limited number of a-values have been published, and the accuracy of these values is rather poor, although precisions reported are quite good. Apparently, systematic errors are involved in the determinations of a-values.

It is interesting to note that the appearance of the term $(\delta\lambda_a^2 + \delta\lambda_s^2)^{1/2}$ in Equation 2 permits an estimate of the ratio $S_A(\Delta\lambda_m)/S_A(\lambda_o)$ of sensitivities obtained with a polychromatic source (D_2 or W lamp) and a line source (HCL), respectively. In the case of the polychromatic source, $\delta\lambda_s$ must be replaced by the spectral band-width of the monochromator $\Delta\lambda_m$. If all other parameters remain constant, we obtain from Equation 2

$$S_A(\Delta\lambda_m)/S_A(\lambda_o) = (\delta\lambda_a^2 + \delta\lambda_s^2)^{1/2}/(\delta\lambda_a^2 + \Delta\lambda_m^2)^{1/2} = \delta\lambda_a/\Delta\lambda_m \tag{25}$$

Typical values of $\delta\lambda_a$ and $\Delta\lambda_m$ for flame AAS are 2 and 500 pm, respectively. Thus the polychromatic beam is absorbed weaker than the monochromatic one by a factor of 4×10^{-3}, and it therefore can be used as reference beam for background correction. Thinking in the reverse sense, a gain in sensitivity by a factor of 250 is achieved by substitution of the polychromatic source by a HCL.[1] On the contrary, the sensitivity of AAS using a polychromatic source can be preselected by choice of $\Delta\lambda_m$. The continuum source AAS will be discussed in Section III.B.

2. Degree of Ionization and Concentration of Free Electrons

In order to achieve the highest sensitivity of determinations by AAS at the atomic or ionic line, the degree γ of ionization should be zero or one, respectively.

$$S_A = (2.315 \times 10^5 \text{cm}/\mu\text{mol})(b/D)(\rho/M_A)\lambda_o G \tag{26}$$

$$G_I \doteq \beta_a(1 - \gamma)\Lambda_I P_I \quad \text{for the atom AI} \tag{27}$$

$$G_{II} = \beta_a \gamma \Lambda_{II} P_{II} \quad \text{for the ion AII} \tag{28}$$

Equation 26 is a simplified form of the sensitivity Equation 2 and has simply been obtained by introduction of a group G of "dimensionless" (or dimension 1) factors β_a, γ, Λ, and P_ℓ ($= P_I$ or P_{II}) which already were defined above. As the new spectroscopic factor Λ (see Equation 21) contains the Gaussian form factor $[2(\ln 2/\pi)^{1/2}]$, the numerical factor of Equation 2 had been increased. The total degree of ionization is γ, and its use is independent of the fact whether only one or more kinds of ions are formed. Nevertheless, the assumption of a single ion A^+ is usually justified by the large difference between the first and second ionization energies, and therefore

$$\gamma = \frac{n(A^+)}{n(A^+) + n(A)} = \frac{1}{1 + n_e/K_I} \tag{29}$$

K_I, the ionization constant (Saha constant), is given by

$$\log K_I = 15.684 + (3/2)\log T + \log Z(A^+,T) - \log Z(A,T) - 5040E_i/T \tag{30}$$

Using theoretical ionization constants calculated from Equation 30 and experimental degrees of ionization (γ), the number density n_e of electrons can be obtained from Equation 29. γ Values are easily determined for the alkaline earth metals Ca, Sr, and Ba as the resonance lines λ_o^I and λ_o^{II} of their atoms and ions, respectively, lie in the visible range of the spectrum. Furthermore, the ionization energies of these metals are low resulting in a measurable ionization in flames, graphite tube atomizers, and in the ICP. If the absorbances A^I and A^{II} are measured for the same concentration c_A of the "indicator element" (Ca, Sr, Ba) with and without added ionization suppressor (e.g., K, Rb, or Cs), γ can be obtained [25] from the following relationship:

$$\gamma_o = (1 - A_s^I/A_o^I)/(A_s^{II}/A_o^{II} - A_s^I/A_o^I) \tag{31}$$

γ_o And γ_s refer to the ionization in the absence and presence of the ionization suppressor, respectively (index "o" and "s", respectively).

$$\gamma_s = (1 - A_o^I/A_s^I)/(A_o^{II}/A_s^{II} - A_o^I/A_s^I) \tag{32}$$

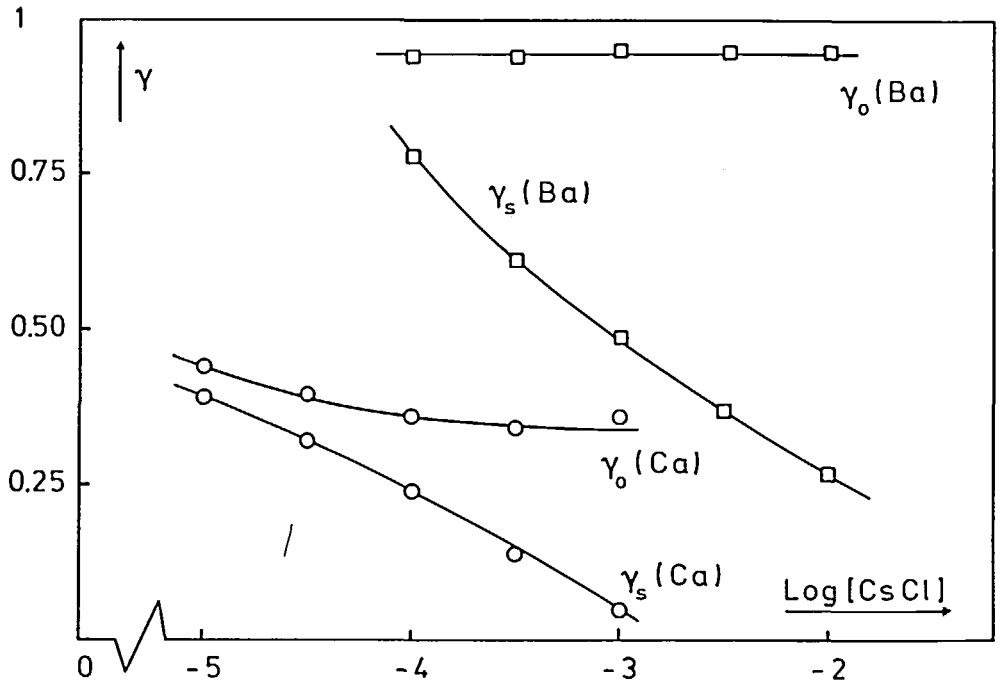

FIGURE 4. Dependence of the degrees γ_o and γ_s of ionization on the concentration [mol/L] of the ionization buffer Cs. γ_o and γ_s refer to the N_2O/C_2H_2-flame without and with CsCl and were obtained from Equations 31 and 32, respectively. Flame conditions are given in remarks to Table 3.

The γ_o value should be independent and γ_s strongly dependent on the concentration c_S of the ionization suppressor (see Figure 4). Whereas the ionization of Ca is suppressed almost completely by 10^{-3} *M* CsCl, concentrations higher than 0.01 *M* in the nebulized solutions would be needed for a complete suppression of the ionization of Ba ($\gamma_s \rightarrow 0$).[26] In both cases the γ_o value is obtained easily by linear extrapolation of the $\gamma_o(c_S)$ values obtained for small concentrations c_S of the suppressor element Cs. The extrapolated values $\gamma_o(c_S = 0)$ may be used for the determination of the number density $n_e(c_A)$ of electrons at a given concentration of the indicator element A (analyte). In order to get n_e for the "unseeded" flame, the $n_e(c_A)$ values whould be extrapolated to $c_A = 0$. The whole procedure is time consuming. Furthermore, the determinations of the absorbances A^I and A^{II} at the same concentration c_A is not possible if the number densities n(A) and $n(A^+)$ are very different in the atomizer in question.

In order to eliminate these drawbacks of the determination of n_e in the "unseeded" absorption volume of the atomizer, the use of sensitivities S_{AI} and S_{AII} will be proposed here. From Equations 26 to 28, one obtains for γ_o (or γ_s) after elimination of factors being the same for the atom and ion.

$$\gamma_o \text{ (or } \gamma_s) = [(S_{AI}/S_{AII})(\lambda_o^{II}/\lambda_o^{I})(\Lambda_{II}P_{II}/\Lambda_I P_I) + 1]^{-1} \quad (33)$$

The initial slopes S_{AI} and S_{AII} of the analytical calibration curves $A_I(c_A)$ and $A_{II}(c_A)$ must be determined under the same experimental conditions using the same atomic absorption spectrometer. No ionization suppressor may be present in the atomizer for the determination of γ_o. On the contrary, γ_s is obtained if an ionization suppressor is present. The advantages of this procedure are

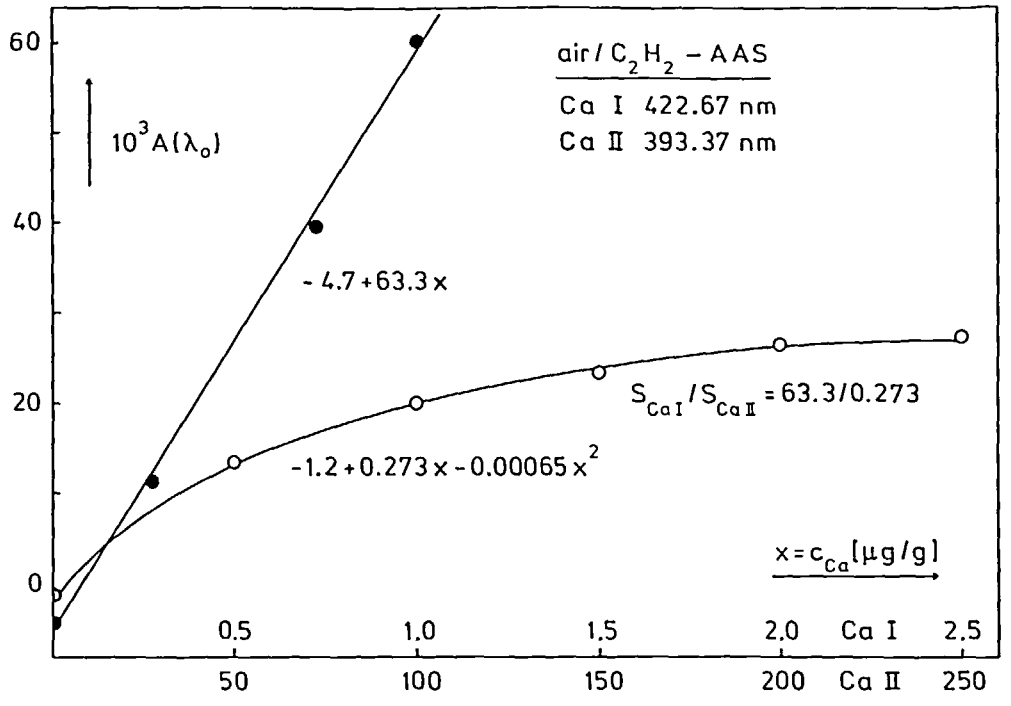

FIGURE 5. Determination of the sensitivity ratio S_{CaI}/S_{CaII} for the air/C_2H_2-flame. Flame conditions are given in remarks to Table 3.

1. A more precise determination of γ_0 (or γ_s) by appropriate choice of the working range is possible.
2. Corrected values of γ_0 for the "unseeded" flame are obtained also in the case of larger curvature of the calibration curves. In that case the sensitivities must be determined by parabolic regression (see Figure 5).

Experimental degrees of ionization obtained by this method are given in Table 3. Although the measured degrees of ionization γ_0 are quite different for the indicator elements used, the same value for the number density of free electrons was obtained for the atomizer in question. Therefore, the average values $\bar{n}_e$ represent the true number densities of free electrons in the "metal free" ("unseeded") atomizers (see Tables 1 and 3). Ba could not be used as indicator element in the air/acetylene flame, because the fraction β_a of Ba atomized, and therefore the number density of BaI and especially that of BaII is very small even at high concentrations of Ba in the nebulized solutions.

The number density of free electrons in unseeded flames is governed by the following reactions:[27]

$$CH + O = CHO^+ + e^- + 84 \text{ kJ/mol}$$

$$CHO^+ + H_2O = H_3O^+ + CO - 209 \text{ kJ/mol}$$

$$H_3O^+ + e^- = H + H_2O - 611 \text{ kJ/mol}$$

Because in the recombination reaction of the ion pair H_3O^+/e^- a large quantity of potential energy is released, the electrons produced in the first reaction are consumed to a high degree

Table 3
IONIZATION DATA OF Ca, Sr, AND Ba FOR THREE DIFFERENT ATOMIZERS

Temperature [K] atomizer	2500 Air/C_2H_2-flame[a]	3000 N_2O/C_2H_2-flame[b]	3000 Graphite-furnace
Ca			
log K_I	8.72	10.90	10.90
S_{CaI}/S_{CaII}	251	1.87	8.20
γ_o	0.0108	0.60	0.253
log n_e	10.65	10.72	11.38
Sr			
log K_I	9.60	11.64	11.64
S_{SrI}/S_{SrII}	28.6	0.52	2.66
γ_o	0.095	0.85	0.53
log n_e	10.58	10.87	11.58
Ba			
log K_I	10.63	12.50	12.50
S_{BaI}/S_{BaII}	—	0.0637	0.326
γ_o	—	0.979	0.90
log $\underline{n}_e$	—	10.84	11.50
log $\bar{n}_e$	10.61	10.81	11.50

Note: Theoretical ionization constants $K_I[cm^{-3}]$ and experimental degrees γ_o of ionization of the indicator elements used for the determination of the number density $n_e[cm^{-3}]$ of free electrons from Equation 29. The γ_o values were obtained from Equation 33 by introducing the experimental sensitivity ratios S_{AI}/S_{AII} for A = Ca, Sr, Ba.

[a] 10 cm slot burner, 15 L/min air and 2.5 L/min C_2H_2, h_o = 6 mm. h_o = observation height.
[b] 5 cm slot burner, 8 L/min N_2O and 5.5 L/min C_2H_2, h_o = 6 mm.

in the last reaction. As a result, small electron concentrations are obtained for both flames and may easily be exceeded by far by analyte contributions. As these electron concentrations are practically the same, the main reactions govern the levels of n_e, which should also be the same in both slightly reducing air/C_2H_2- and N_2O/C_2H_2-flames (see remarks to Table 3).

The number density of the free electrons in the graphite furnace atomizer is much higher than those in the N_2O/C_2H_2-flame at about the same temperature of 3000 K. Apparently, the thermionic emission of electrons from the graphite surface provides electrons at a relatively fast rate, and there is no such effective electron trap reaction in the furnace protected by N_2 (or Ar) as the last reaction mentioned above.

The number density of free electrons inside the unloaded furnace has to be known in order to be able to apply the Saha equation to ionization equilibria: $A = A^+ + e^-$. "There are, unfortunately, no reports available on ionization processes in constant-temperature furnaces and only a limited number of studies dealing with ionization in pulse-heated electrothermal "ET" atomizers." This was ascertained by Matousek[28] some years ago. Sturgeon and Chakrabarti[29] estimated the equilibrium concentration for the reaction $C_n(s) = C_n^+(s) + e^-$ from the thermionic emission equation[30]

$$(n_e)_{eq} = [2(2\pi m_e kT)^{3/2}/h^3]\exp(-\phi/kT) \quad (34)$$

where m_e is the electron mass and h the Planck constant. The other symbols have their usual meaning and were already introduced above. These authors obtained $10^{13.18}$ cm^{-3} for 3000 K. This equilibrium value is markedly higher than the experimental value of $10^{11.50}$ cm^{-3} obtained in this work (see Table 3), which is in excellent agreement with the values derived by Littlejohn and Ottaway[31] from ionization temperature measurements in a Perkin-Elmer HGA-72 graphite tube atomizer: $10^{10.72}$ cm^{-3} and $10^{11.11}$ cm^{-3} at 2558 K and 2766 K, respectively. Higher values were obtained by Sturgeon et al.:[32] $10^{11.40}$ cm^{-3} and $10^{12.89}$ cm^{-3} at 2470 K and 3000 K, respectively. These authors measured the attenuation of microwave radiation by free electrons in a Perkin-Elmer HGA-2200 graphite tube atomizer.

These relative small deviations between experimental values obtained by different methods may at least partly be due to the different coverages of the graphite surfaces by impurities influencing the thermionic work function ϕ. Furthermore, the local concentration of electrons varies along the axis and the radius of the tube, presumably. Therefore, the geometry of the measuring beam should be the same as for the hollow cathode radiation and the microwave radiation. This was certainly not the case.

The characteristic values of n_e for the flames and graphite tube should be used carefully. The value for the nitrous oxide acetylene flame seems to be the best defined one, because it is practically independent of the oxidant to fuel ratio F_{ox}/F_{fu}. On the other hand, n_e for the air/acetylene flame enhances from $10^{10.61}$ to $10^{11.4}$ if F_{ox}/F_{fu} is changed from 6.0 (see Table 3) to 4.8 corresponding to a strongly reducing air/acetylene flame. This enhancement is caused by the thermionic emission of electrons from the small graphite particles produced in the flame.[33] The rate of emission of electrons from positively charged particles can be expressed as

$$j = BT^2 \exp\left[\frac{-e}{kT}\left(\phi + \frac{eN}{r_p} + \frac{e}{2r_p}\right)\right] \tag{35}$$

The preexponential term B, like the work function ϕ, is characteristic for the material. These values are 48 A/cm² and 4.4 V in the case of electrons, which left the particle of small finite radius r_p. In the case of a bulk material, e.g., the graphite tube of the atomizer, r_p is practically infinite and the second and third terms representing the attraction of the leaving electron by the positive charging and the induced dipole of the material, respectively, must be canceled. The number of electrons emitted by 1 cm² of soot particles in a second ($\propto$ j) may be strongly influenced by elements providing refractories on their surface, because these materials often have low work functions, e.g., 1.7 V in the case of BaO. Furthermore, there is very little information available on the number size distributions of soot particles, which makes predictive calculation of j very tentative.[33] Therefore, the results of the n_e measurements by AAS should be compared with experimental values obtained by other independent methods.[33] Unfortunately, no numerical values for the "characteristic electron concentrations" in unseeded analytical flames have been presented in the most comprehensive works[2,33,34] about flames.

The determination of the degree of the ionization γ_o of Sr and Ba in the ICP could not be carried out as the atomic emission of these elements in the ICP exceeded their emission from the corresponding hollow cathodes, and therefore no atomic absorption could be measured. According to the higher excitation energies (shorter wavelengths) of CaI and CaII, the degree of ionization of CaI could easily be measured in ICP by AAS. Nevertheless, γ_o also depends strongly on the volume flow rates of the ICP. As a consequence, the effective temperature in the absorption volume of the ICP would be required for the calculation of the Saha constant, which must be known for the calculation of n_e using the Equation 29. However, temperature measurements in the ICP[35] were beyond the scope of this work.

3. Degree of Dissociation

Since the Equations 2 and 26 to 28 remain valid regardless of the number of chemical reactions occurring in the atom reservoir, the use of the atomized fraction β_a in place of the degree β_d of the dissociation defined for a given chemical reaction AX = A + X is preferred here. If only a single chemical reaction and a single ionization occur, β_a can easily be calculated:

$$\beta_a = \frac{n(A) + n(A^+)}{n_t} = \frac{1}{(1 - \gamma)/\beta_d + \gamma} \tag{36}$$

If no ionization occurs ($\gamma = 0$), β_a and β_d are identical. Using β_a instead of β_d means that the ion A^+ is considered as a chemically dissociated species. This is a reasonable point of view. The β_d can be obtained from the dissociation constant K_d if the number density n_X of the dissociation product X is known:

$$\beta_d = \frac{n(A)}{n(A) + n(AX)} = \frac{1}{1 + n_X/K_d} \tag{37}$$

Statistical thermodynamics provide the following term for the dissociation constant K_d:

$$K_d = \frac{n_A n_X}{n_{AX}} = \frac{Z_A(T)Z_X(T)}{Z_{AX}(T)} \left(\frac{m_A m_X}{m_{AX}}\right)^{3/2} \left(\frac{2\pi kT}{h^2}\right)^{3/2} \exp(-D_o/kT) \tag{38}$$

The mass of the particle given as an index of m is m, h is the Planck constant, and D_o is the bond dissociation energy. As D_o is in the range of 1 to 10 eV and independent of the temperature, the last three equations allow one to make the general statement that all compounds AX dissociate completely if the temperature of the atomizer is high enough to have $K_d \gg n_X$. In that case β_d and β_a approach one. Nevertheless, the use of these equations for the estimation of β_d is rather difficult. On the other hand, the combination of the Equations 37 and 38 provides a useful interpolation formula, e.g., for the dissociation of the monoxides AO in the N_2O/C_2H_2-flame:[6]

$$y = \log\left[\left(\frac{1}{\beta_d} - 1\right)\left(\frac{M_A}{M_{AO}}\right)^{3/2} Z_A(T)\right] = y_o + 5040\,\frac{D_o}{T} \tag{39}$$

$$y_o = \log n_O - \log\left[\left(\frac{2\pi kTm_O}{h^2}\right)^{3/2} \frac{Z_O(T)}{Z_{AO}(T)}\right] \tag{40}$$

As the ratio $Z_O(T)/Z_{AO}(T)$ of the partition functions of the atomic oxygen and the different metal monoxides AO is not strongly dependent on the kind of A and the temperature T and also the number density n_O of the oxygen atoms remain about the same for similar flame conditions, the term y_o remains constant to a first approximation. As a consequence, a simple linear relationship between y and D_o is obtained (see Figure 6). The square r^2 of the correlation coefficient r of the linear regression line is only 0.987, indicating a rather poor precision. The relatively large scatter of the points is caused to a great degree by the uncertainties of the experimental values[21] of β_d needed for the calculation of the new variable y.[6] These have arisen because the composition of the flames used for the determination of the β_d values was somewhat different. Additionally, the observation height was also not always the same. Nevertheless, the regression line of Figure 6 is useful for estimations of β_d values, because many bond dissociation energies[2,22] but only a limited number of β_d values are known.

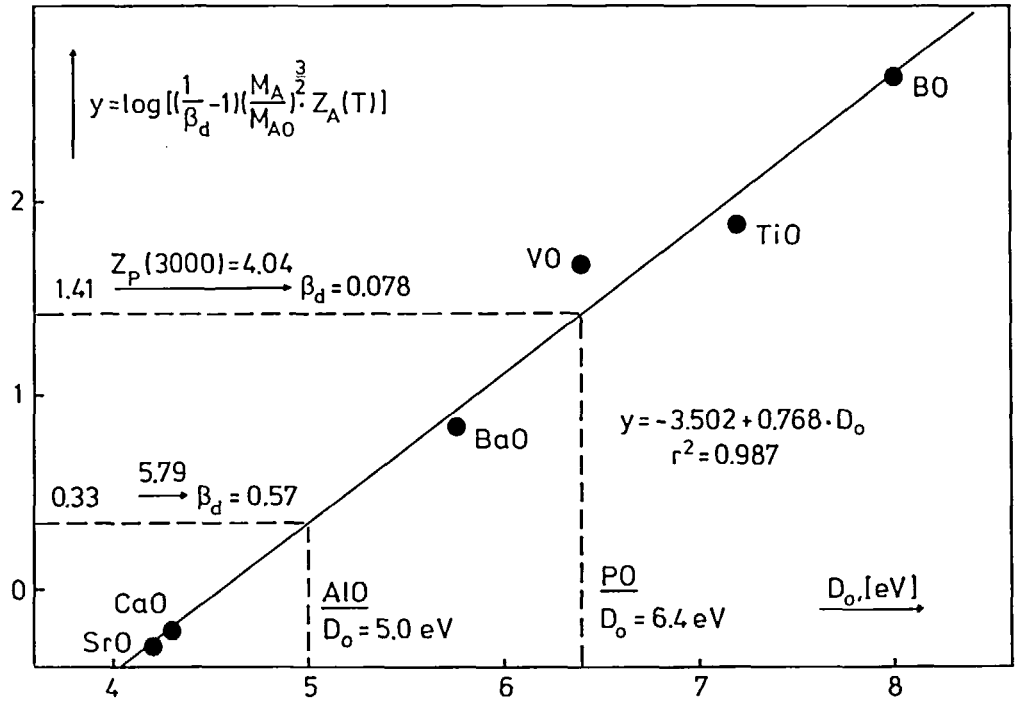

FIGURE 6. Estimation of the degree of dissociation of phosphorus monoxide and aluminium monoxide in the nitrous oxide/acetylene-flame using the semi-empirical relationship Equation 39. In the term y, β_d is the degree of dissociation, M the relative mol mass of the analyte atom A and its monoxides AO, and Z_A the electronic partition function of A. D_o is the bond dissociation energy of the monoxides, and r^2 is the square of the correlation coefficient of linear regression of y on D_o.

The β_d value of 0.57 obtained for AlO from Figure 6 is more than twice the average value of 0.23 calculated from the valuable compilation of Kirkbright and Sargent.[21] Nevertheless, the agreement may be considered as good, because the degrees of atomization are generally reliable within a factor of two[36,37] and because the estimate of β_d from Figure 6 depends strongly on the bond dissociation energy D_o selected. Namely, if the value of 5.5 eV, which was adopted by Alkamade et al.[2] for the construction of diagrams "association factor [A]/[AO] vs. reciproke temperature $^1/T$," is used for the interpolation in Figure 6, an estimate of 0.29 for β_d of AlO is obtained. No comparison of the estimate for PO with literature data is possible at the present time because no measured dates are available.

C. Comparison of Theoretical and Experimental Sensitivities

1. Problems Involved in Calculation of Theoretical Sensitivities

The simplified form (see Equation 26) of the sensitivity Equation 2 involves two factors (G and D) that are the main origin for the uncertainties of theoretical sensitivities. In the group G of dimensionless factors, the fraction atomized, β_a, reveals the largest uncertainty. Therefore, β_a values are given only to one decimal number in the *CRC Handbook of Spectroscopy*.[38] The dilution factor D depends on the volume flow rates F_ℓ, F_{fu}, F_{ox}, and the efficiency ϵ_n of the nebulization (see Equation 17). Unfortunately, the estimation of ϵ_n from the rate of liquid consumption F_ℓ and the backflow F_b (see Section II.A.2) is a simple but an inaccurate method. This indirect method is prone to significant systematic errors because of its sensitivity to even very small recovery losses. Generally, indirect methods of transport efficiency measurements (ϵ_n measurements) are inherently inaccurate, particularly for low transport efficiency.[39] Direct ϵ_n measurements, relying upon solvent collection, are

again inherently inaccurate as a consequence of evaporation processes that occur in the spray chamber.

The only reliable technique for transport efficiency measurements, particularly for low transport efficiency, requires a direct collection of the analyte.[40] The collection of the aerosol must be carried out with the burner in its place and with volume flow rates used for the measurements of absorbances. The efficiency of nebulization ϵ_n, used in this work, was determined[41] by collection of HNO_3 from the aerosol produced from 0.1 *M* HNO_3. Introducing ϵ_n into the Equation 17, precise values for the dilution factor D_f result. Nevertheless, the sensitivities calculated from Equation 26 using these D_f-values are generally too high because the analyte losses, which occur in the flame, are not taken into account. In order to account for that, not ϵ_n but the product $\epsilon_n\beta_s\beta_v$ should be introduced into Equation 17. "The fraction desolvated, β_s, is the ratio of the amount of the analyte passing in the desolvated state to the total amount of analyte passing." The fraction volatilized, β_v, is "the ratio of the amount of analyte passing into the gaseous state to the total amount of analyte passing in the desolvated state." These definitions[42] of IUPAC are very useful for classification of "side reactions" that may reduce the number density of atoms in the absorption volume. Nevertheless, they are of little use at the present time for the calculation of sensitivities because no method exists for their determination or calculation.

The concept of "useful mass transport rate" W_u proposed by Browner et al.[43] has more practical importance in this sense.

$$W_t = W_u + W_e = \sum_{d_i=0}^{d_{max}} \left(\frac{\partial W}{\partial d}\right)_i \Delta d_i + \sum_{d_{max}}^{d_i=\infty} \left(\frac{\partial W}{\partial d}\right)_i \Delta d_i \qquad (41)$$

The total and excess mass transport rates [μg/s] are W_t and W_e, respectively. The maximum droplet diameter is d_{max} and is defined such that only droplets equal to or smaller than this diameter contribute significantly to the analytical signal, e.g., 90% of the analytical signal is due to that part of analyte which is transported in droplets of the diameter $0 < d_i < d_{max}$. The droplet size distribution ($\partial W/\partial d$), which is a function of d_i, can be determined from cascade impactor data.

Whereas the calibration function "$A(\lambda_o)$ vs. W_t" was strongly bent for the Ca 422.6 nm line and the air/acetylene flame as atomizer, the calibration function "$A(\lambda_o)$ vs. W_u" remained linear in the same range of the total mass transport rate[43] ($20 < W_t < 80$ μg/sec). Nevertheless, the use of W_u as a new independent variable in the place of the concentration c_A has very little chance to be generally accepted because the determination of d_{max} from the droplet size distribution "($\partial W/\partial d$) vs. d_i" is a time consuming procedure. Another possibility would consist in the correction of the dilution factor D_f by its multiplication with W_t/W_u. This was not tried at the present time because a much simpler procedure was developed recently[41] for the determination of the dilution factor, which accounts for analyte losses due to incomplete desolvation and vaporization ($\beta_s\beta_v < 1$). This procedure is described in the following section.

2. *Determination of the Dilution Factor D_i by the Ionization Suppression Method*

The dilution factor D_f is defined by Equation 17, whereby the efficiency ϵ_n of nebulization, measured by direct collection of the analyte, should be used. For the determination of a correct dilution factor $D_f/\beta_s\beta_v$, the measurements needed must provide the information from the absorption volume of the atomizer. As the determination of the number density of electrons in unseeded flames and in flames seeded with Cs has revealed to be a simple and straightforward procedure (see Section II.B.2), it was thought that this procedure should be used for the determination of the dilution factor D_i, which should represent $D_f/\beta_s\beta_v$. As the ionization of Cs is practically 100%, D_i is given by the number density $(n_{Cs})_s$ of Cs in the

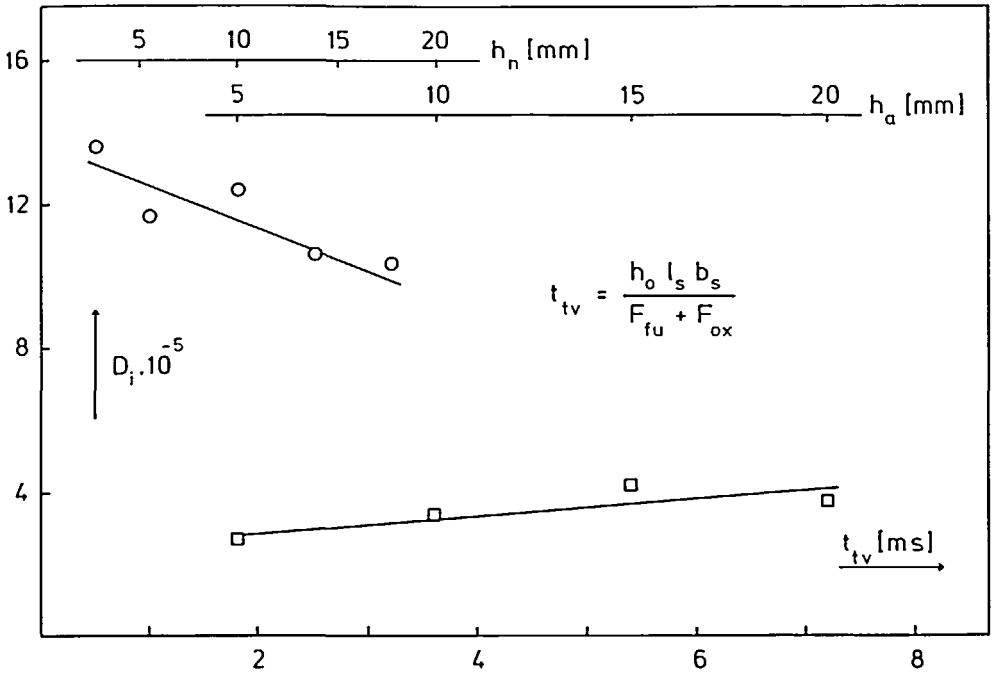

FIGURE 7. Dependence of the dilution factor D_i, determined by the ionization suppression method (see Section II.C.2) on the travel time,[42] t_{tv}, and on the observation height h_n for the nitrous oxide acetylene flame (see circles), and h_a for the air acetylene flame (see squares), respectively. Calculated from the term given in this figure was t_{tv}. The length and the width of the slit are l_s and b_s, respectively. The volume flow rates of the fuel and the oxidant are F_{fu} and F_{ox}, respectively. Weakly reducing flames were used (see captions to Tables 4 and 5).

solution divided by the enhancement $(\Delta n_e)_a$ of the number density of free electrons in the absorption volume of the atomizer due to the addition of the ionization suppressor CsCl. Using Equation 29, $(\Delta n_e)_a$ [$= (n_e)_s - (n_e)_o$] can easily be replaced by the degrees γ_s and γ_o of ionization on the indicator element (Sr) in the flame with and without the ionization suppressor (Cs):

$$D_i = \frac{(n_{Cs})_s}{(\Delta n_e)_a} = \frac{6.022 \times 10^{20}[Cs]}{K_I(1/\gamma_s - 1/\gamma_o)} \tag{42}$$

On principle, four sensitivities must be measured for the determination of D_i: from the sensitivities S^o_{SrI} and S^o_{SrII}, measured at the atomic and ionic line of strontium in the unseeded flame (index "o"), γ_o is obtained according to Equation 33, and from the sensitivities S^s_{SrI} and S^s_{SrII}, measured at the atomic and ionic line of strontium in the seeded flame (index "s"), γ_s is obtained according to the same Equation 33. In the case of the N_2O/C_2H_2-flame, γ_o is practically independent of the ratio of the volume flow rates F_{ox}/F_{fu}. Therefore, γ_o can be considered as constant and only the sensitivities S^s_{SrI} and S^s_{SrII} must be measured for the determination of D_i. In the air/acetylene flame, γ_o depends on the ratio of the volume flow rates. Therefore, γ_o must be measured for different ratios.

In Figure 7 the dependence of D_i on the observation height h_o is shown. As the concentration of the electrons varies with h_o, γ_o and γ_s were measured at each observation height.[41] The dilution factor D_i should slightly increase with increasing observation height because of the expansion of the flame. Indeed, a small increase of D_i was obtained for the air/acetylene flame in the range of 5 to 20 mm. On the contrary, a small decrease of D_i seems to occur in the nitrous oxide/acetylene flame. This unexpected result may be due to inhomogenity

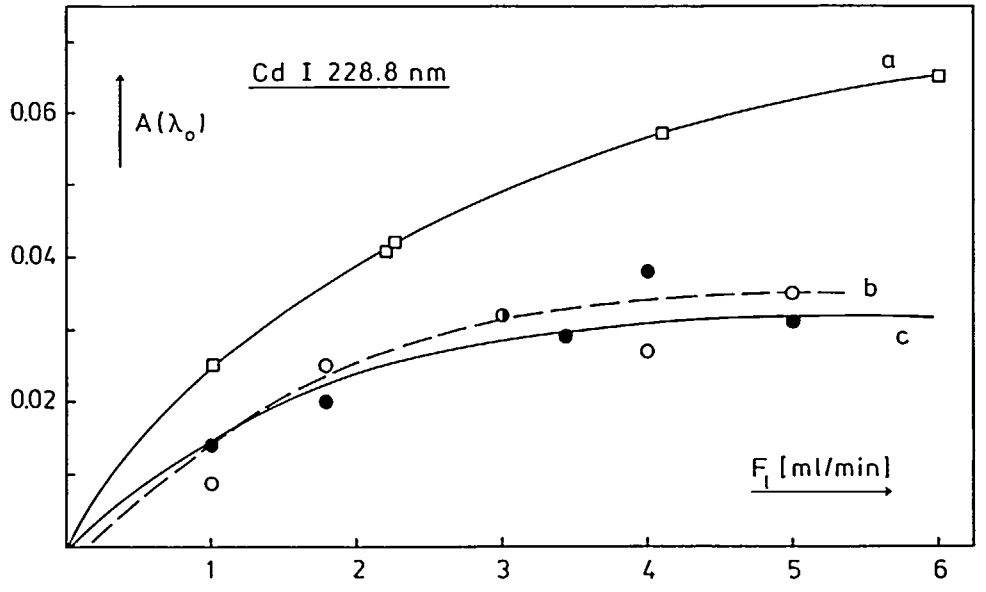

FIGURE 8. Comparison of calculated and measured absorbances $A(\gamma_o)$ in the function of the liquid aspiration rate F_ℓ: (a) calculated as $S_{Cd} \cdot c_{Cd}$, using dilution factors D_ℓ, determined according to its definition (see Equation 17); (b) calculated as $S_{Cd} \cdot c_{Cd}$, using dilution factors D_i, determined by the ionization suppression method (see Section II.C.2); and (c) measured absorbances (see dots). S_{Cd} is the theoretical sensitivity for the determination of Cd by AAS, and it was calculated from Equation 26. The concentration c_{Cd} was 1 μg/g. The half-filled circle represents both a calculated (b) and a measured (c) absorbance value. An oxidizing air/acetylene flame was used (see caption to Table 5).

of this flame. The travel time,[42] t_{tv}, is the time needed for the substance to be carried from the base of the flame to the observation volume. t_{tv} Is a very valuable quantity because it involves all the most important constructional characteristics of the burner/atomizer system: slot length l_s, slot width b_s, the volume flow rates F_{fu} and F_{ox}, and also h_o (see Equation in Figure 7). The use of t_{tv} makes the rational characterization of the burner/flame system possible. Additionally, t_{tv} is a concept easy to imagine, therefore, it should be used much more than it has been up to now.

In Figure 8 the absorbances $A(\lambda_o)$, measured at different liquid consumption rates F_ℓ (see full circles), are compared with calculated absorbances $S_{th} \cdot c_{Cd}$ whereby c_{Cd} is the concentration of cadmium standard solution nebulized. Using the theoretical sensitivity S_{th}, obtained with the dilution factor D_ℓ, practically no deviations from the smooth curve (a) are obtained, because D_ℓ can precisely be obtained from Equation 17 using efficiencies ϵ_n measured by the method of direct analyte collection. Nevertheless, the calculated absorbances are systematically too high. Using the sensitivity S_{th}, obtained with D_i, the calculated absorbances (see empty circles) show a relatively large scatter, but they are in good agreement with the measured values. The scatter of the calculated absorbances is due to a relatively large standard deviation of D_i values determined at different liquid consumption rates F_ℓ. Namely, there are four sensitivities measured at relatively small concentrations of Sr. This results in a relatively large propagated SD of D_i. Nevertheless, it is better to have less precise but correct estimates for the theoretical sensitivities than those being precise but inaccurate.

The advantage of the use of D_i for the estimation of theoretical sensitivities are

1. D_i is "measured" in the absorption volume of the atomizer and therefore accounts for analyte losses in the flame. As the fraction β_s of the analyte desolvated mainly depends on the properties of the solvent, D_i accounts completely for $\beta_s < 1$. On the contrary,

the fraction β_v of the analyte vaporized, mainly depends on the properties of solute. Therefore, D_i may be somewhat over or under compensated for $\beta_v < 1$.

2. The determination of D_i is a fast procedure in comparison with the determination of D_f by the direct analyte collection, including calibration of flow meters. D_i can conveniently be obtained by using a two-channel AA-spectrometer. The simultaneous measurements of the sensitivities of SrI and SrII also provide a somewhat better accuracy for D_i.

3. Comparison of Theoretical and Experimental G-Values

The comparison of theoretical and experimental sensitivities may be transformed to the comparison of the theoretical and experimental G-values (see Equations 26 to 28). Whereas the comparison of sensitivities is always limited to a given experimental setup, the comparison of G-values is released from this "ballast" and therefore will be preferred here. Although the individual factors of G, e.g., β_a and γ, were discussed in detail in the original literature, their combined effect upon the sensitivity of determinations by AAS has never been studied systematically. Only a limited number of theoretical sensitivities have been calculated.[5,6,7] The aim of this comparison is to answer the question whether the "theoretical" G-values, calculated from literature data, are good enough for calculation of sensitivities or whether the G-values should be determined using the new ionization suppression method for the measurement of "experimental" G-values.

The theoretical G-values, G_{th}, were calculated according to their definitions by Equations 27 and 28. The fraction β_a of the analyte atomized was taken from the *CRC Handbook of Spectroscopy*.[38] If no β_a value was available for an element in question, β_d was calculated from the following equation

$$(\beta_d = \beta_a \text{ for } \gamma = 0)$$

$$\beta_d = [10^y/(Z_A(T) \times (M_A/M_{AO})^{3/2}) + 1]^{-1} \quad (43)$$

The variable y for the nitrous oxide/acetylene flame was calculated from the regression equation given in Figure 6 using the bond dissociation energies D_o of Table 2. The regression equation for the air/acetylene flame was calculated by using the β_a and D_o values for Ba, Ca, Co, Cr, Fe, In, Mn, Sn, and Sr compiled in Table 2: $y = -2.76 + 0.928 \cdot D_o$. The square of the correlation coefficient amounted to 0.661, indicating a poor correlation. Therefore, the calculated values from Equation 43 marked with a star, must be regarded as rough estimates. The degrees γ of the ionization were determined experimentally (see Equation 33) in the case of the alkaline earth metal Ca, Sr, and Ba. In the other cases, γ was calculated from Equation 29 using theoretical Saha constants K_I (see Equation 30) and number densities of free electrons for the corresponding flame (see Tables 1 and 3). These γ-values are therefore valid for $n(A^+) \ll (n_e)_a$ where $n(A^+)$ is the number density of the analyte cations. Of course, this criterion is always fulfilled for the limiting value $c_A \rightarrow 0$. The calculation of the remaining two factors P_ℓ and Λ of the cluster G were already discussed in detail in Section II.B.1.

The experimental G-value is obtained by setting the measured sensitivity S_{ex} into the Equation 26 and solving this for G ($= G_{ex}$):

$$G_{ex} = S_{ex}[2.315.10^5 \text{ cm}/\mu\text{mol})(b/D_i)(\rho/M_A)\lambda_o]^{-1} \quad (44)$$

All symbols of this term were explained above (see Equations 2 and 26). The absorption path length b may be set equal to the slot length (10 cm) in the case of the burner for the air/acetylene flame. In the case of the burner used for the nitrous oxide/acetylene flame, b

Table 4
COMPARISON OF THEORETICAL AND EXPERIMENTAL G-VALUES FOR THE NITROUS OXIDE/ACETYLENE FLAME (3000 K)

Analyte/ class	β_a [1]	γ [1]	Λ [10^5]	P_ℓ [1]	G_{th} [10^3]	G_{ex} [10^3]	G_{ex}/G_{th} [1]
Ag/a	0.6	0	2.00	0.501	60	49.7_o	0.83
Al/c	0.2	0.27	0.697	0.169	2.3	2.78_r	1.21
As/c	0.6*	0	0.864	0.247	13	14.5_r	1.12
Au/a	0.5	0	1.60	0.483	39	31.6_o	0.81
B/c	4.10^{-3}	0	0.117	0.168	0.008	0.075_{sr}	(9.4)
Ba/c	0.2	0.98	3.59	0.824	1.2	1.39_r	1.16
Ba^+/c	0.2	0.98	3.43	0.360	24	31.9_r	1.33
Ca/c	0.5	0.55	2.38	0.994	53	55.0_r	1.04
Ca^+/c	0.5	0.55	1.86	0.497	25	30.2_r	1.21
Cd/a	0.6	0	2.90	1.00	170	186_o	1.09
Co/a	0.25	0	3.73	0.0404	3.8	29.0_o	(7.6)
Cu/a	0.7	0	1.52	0.492	52	35.6_o	0.69
Cr/c	0.6	0.08	4.01	0.131	31	32.0_r	1.03
Eu/c	0.4*	0.92	10.89	0.123	54	37.6_r	0.70
Fe/a	0.8	0	8.25	0.0455	30	30.6_o	1.02
Hg/a	1	0	0.112	1.00	11	2.03_o	(0.18)
Mg/a	1.0	0	1.98	1.00	200	115_o	0.58
Mn/a	0.8	0	5.65	0.162	73	58.4_o	0.80
Mo/a	0.7*	0	2.95	0.140	29	37.2_r	1.28
Ni/a	1.0*	0	10.4	0.0379	39	16.5_o	0.42
Pb/a	0.8	0	0.639	0.990	47	29.3_o	0.62
Pd/a	1.0*	0	0.225	0.681	15	12.4_o	0.83
Pt/a	1.0*	0	2.59	0.0593	15	4.01_o	(0.27)
Se/c	0.9*	0	1.16	0.154	16	10.3_o	0.64
Si/c	0.06	0	0.671	0.110	0.44	2.71_{sr}	(6.2)
Sn/c	0.8	0	0.866	0.296	17	18.2_r	1.07
Sr/b	0.3	0.93	3.73	0.996	7.8	10.0_r	1.28
Sr^+/b	0.3	0.93	2.80	0.497	39	63.7_r	1.63
Ti/c	0.2	0.15	1.98	0.0438	1.7	2.57_r	1.51
Zn/a	0.9	0	2.61	1.00	240	241_o	1.00

Note: a, b, c = spectrochemical classes (for classification see legend to Table 2), β_a = fraction of analyte atomized[38] (values marked with a star were calculated from Equation 43 using the bond dissociation energies D_o of Table 2), γ = degree of ionization, Λ = spectroscopic factor, P_ℓ = population factor, G_{th} and G_{ex} = theoretical and experimental cluster of dimensionless factors (see Equations 26 to 28). The redox-property of the flame used for the determination of G_{ex} is indicated by an index attached to the corresponding G_{ex}-value: "o" oxidizing (1.9), "r" reducing (1.6), and "sr" (1.3) strongly reducing. The ratio (F_{ox}/F_{fu}) of the volume flow rates are given in parentheses. The observation height was 10 mm above the slit of 5 cm length.

was markedly shorter than the slot length (5 cm). Therefore, b was measured in the following way: a little MgO-rod was blackened by a pencil lead, and it was kept into the flame at the observation height in question for a short time. The length of the MgO-rod, at which it was cleaned by volatilization of graphite, was taken as the absorption path length b.

The theoretical and experimental G-values are given in Tables 4 and 5 for the N_2O/C_2H_2-flame and the air/C_2H_2-flame, respectively. Because the fraction β_a of analyte atomized is generally reliable within a factor of 2,[36,37] ratios G_{ex}/G_{th}, smaller than about 0.5 and greater than about 2, may be considered as runaways, e.g., Co and Pt in both flames. In that case, the spectroscopic factors Λ may have systematic errors due to incorrect weighted oscillator

Table 5
COMPARISON OF THEORETICAL AND EXPERIMENTAL G-VALUES FOR THE AIR/ ACETYLENE FLAME (2500 K)

Analyte/ class	β_a [1]	Λ [10^5]	P_ℓ [1]	G_{th} [10^3]	G_{ex} [10^3]	G_{ex}/G_{th} [1]
Ag/a	1.0	2.13	0.501	110	50.2	0.46
Au/a	1.0	1.70	0.494	84	58.1	0.69
Cd/a	0.5	3.11	1.000	160	146	0.91
Co/a	0.3	4.02	0.0456	5.5	35.0	(6.4)
Cu/a	1.0	1.63	0.499	81	38.0	0.47
Fe/a	0.4	8.87	0.0482	17	51.9	(3.05)
Hg/a	1	0.122	1.000	12	1.36	(0.11)
In/b	0.6	1.76	0.320	34	6.76	(0.20)
K/b[a]	0.4	1.74	0.500	30	38.3	1.28
Mg/a	0.6	2.13	1.000	130	114	0.88
Mn/a	0.6	6.06	0.165	60	44.4	0.74
Na/b	1.0	1.39	0.501	70	38.0	0.54
Ni/a	0.7*	11.2	0.0404	32	24.1	0.75
Pb/a	0.7	0.676	0.959	46	20.9	0.45
Pd/a	0.8*	0.241	0.807	16	24.2	1.50
Pt/a	0.8*	2.75	0.0626	14	4.96	0.35
Rb/b[a]	1.0	2.33	0.500	82	33.0	0.40
Sr/b	0.075	3.92	1.002	24	22.8	0.95
Tl/b	0.5	1.86	0.488	45	18.5	0.41
Zn/a	0.7	2.82	1.000	200	219	1.10

Note: a, b = spectrochemical classes (for classification see legend to Table 2), β_a = fraction of analyte atomized[38] (values marked with a star were calculated from Equation 43 using the bond dissociation energies of Table 2), Λ = spectroscopic factor, P_ℓ = population factor, G_{th} and G_{ex} = theoretical and experimental cluster of dimensionless factors (see Equations 26 to 28). G_{ex}-values were determined in the oxidizing flame with ratios (F_{ox}/F_{fu} of the volume flow rates of 6-7. In the case of Sr a reducing flame with F_{ox}/F_{fu} of 5.3 was used. The observation height was 10 mm above the slit of 10 cm length. Solutions of metals of class b contained 0.01 *M* CsCl.

[a] Degree of ionization γ_s = 0, except: K 0.17 and Rb 0.30.

strengths (gf). Indeed, these (gf)-values were taken from an old compilation[44] containing a greater number of (gf)-values that had been corrected in more recent works.[22,45] The incorrect (gf)-value may also contribute to a large degree to the overestimation of G_{th} of Hg for both flames. In the case of metals, having very strong monoxides, e.g., B and Si, the degree of dissociation β_d ($\simeq \beta_a$ in these cases) is very strongly dependent on the oxidant-to-fuel ratio. Apparently, this was not sufficiently small in the experiment carried out for the determination of β_a. As a consequence, the G_{th}-values are underestimated in respect to G_{th}-values for strongly reducing flames used for the determination of the G_{ex}-values in this work (see Table 4). In the case of Fe and In both critical factors β_a and (gf) may contribute to the under- and overestimation of G_{th}, respectively, for the air/acetylene flame.

If the uncertain values just discussed and which have been set in parentheses in Table 2 are omitted, the average value (G_{ex}/G_{th}) of 0.996 ± 0.301 (SD) is obtained from the 25 ratios. As the deviation of the average value from the ideal value of 1 is very small, the new ionization suppression method for the determination of the dilution factors provides accurate D_i values, which is the requirement for obtaining accurate G_{ex}-values from Equation

44. On the other hand, the SD is large. This is caused partly by the uncertainties of the factors β_a and Λ of the G_{th}-term (see Equations 27 and 28) and partly also by the SD of the dilution factor D_i, which is propagated into the G_{ex}-values.

The average value $(G_{ex}/G_{th})_{av}$ calculated from the 16 values in the last column of Table 5 is 0.74 ± 0.34 (SD). This SD corresponds to a confidence interval of the mean of 0.17 at the 95% confidence level. Therefore, the relatively small systematic deviation of the average value from the ideal value of 1 is significant at the 95% confidence level. This lower $(G_{ex})_{av}$-value might be due to the lowering of the number density of analyte atoms by their recombination to molecules in the boundary zones of the unshielded air/acetylene flame used for the determination of the G_{ex}-values. Thus, this flame is less suitable than the nitrous oxide/acetylene flame for standardless or absolute analysis by AAS (see next section). For this purpose, the use of G_{ex}-values is recommended because they are more precise and accurate than the G_{th}-values.

D. The Possibility of Standardless AAS

"The history of modern spectrochemistry is essentially the history of continuous search for analytical methods requiring no standards and in which the compositions of samples have no effects on the results of the analysis." This profound conclusion was written by L'vov in 1970.[10] Other statements of his are also very important in this sense, e.g., "in spite of the comparatively long and thorny path which emission spectroscopy has followed in pursuing this line, a general solution of the problem of spectrochemical analysis without using standards has not yet been found" but "atomic absorption analysis not using standards will be introduced in the near future" and "the cuvette will be best in . . . analysis without standards."

Nevertheless, 15 years more were necessary for the development of the graphite furnace technology in order to achieve an accuracy of 10 to 20% by standardless furnace AAS.[46] This time can be divided in three stages,[47] which may be characterized by the change of the number (N) of publications in the field of furnace AAS per year. In the first period of 1970 to 1974, $\Delta N/\Delta Y$ was about +55/y. The rapid growth in these years can be attributed to the appearance of commercial equipment and a rapidly rising interest in this sensitive method. The stagnating interest in the second period as measured by the small "slope" of only ca. +3/y may be explained with the realization of limitations of the furnace technique of AAS. From 1980 a new stage of enthusiasm was indicated by the slope of 23/y corresponding to 10% increase in the number of publications per year. This is stimulated by improvements in the atomization techniques that have removed or alleviated the limitations of the furnace AAS.

The difficulties encountered in the application of furnace AAS originated from the use of transient absorption signals arising from atomic absorption in the atomizer zones which were not isothermal in time and space. Three approaches were tried:[47] (1) heating of the furnace by capacitive discharge, (2) using the probe technique, and (3) using the platform. Of these techniques, the sample vaporization from the platform has enjoyed the widest use since it does not require any modification in furnace design or measurement procedure. Because the temperature of the platform, which may be a section of a tube placed below the injection hole, lags behind that of the furnace, sample vaporization from the platform occurs in an environment of higher temperature. Therefore, the atoms produced do not recombine to clusters or even to refractories. The most significant development in this method has become the concept of the "stabilized temperature platform furnace" (STPF) that fulfills the requirements for standardless furnace AAS. The possibility of this technique was recently discussed by Slavin and Carnrick.[46]

STPF technology includes more than just the L'vov's platform for it to work as well as necessary for standardless furnace AAS,[46] e.g., modern furnaces with separate controls for

heating rate and final temperature, Zeeman background correction providing fully background-corrected readings every 20 msec, and the use of integrated absorbance signals. The standardless furnace AAS is based on the stability and transferability of characteristic masses m_o which is a measure of the sensitivity for a particular analyte when the furnace technique is used. The mass in pg that produces an integrated absorbance signal equivalent to 0.0044 absorbance units is m_o. From the m_o values, obtained for different matrixes in three different Perkin-Elmer laboratories, the following average m_o values and SD of the single values have been calculated: Cd $0.37 \pm 0.05_{11}$, Al $10 \pm 4_{11}$, As $15 \pm 2_5$, Pb $11 \pm 2_7$, Se $28 \pm 9_8$, and Tl $9.5 \pm 1.0_6$. The number added to SD as an index gives the number of independent m_o values used for the calculation of the mean and the SD. The characteristic mass data seem to be very stable and relatively invariant among instrument as long as similar experimental conditions are used, such as the same furnace design, char and atomization temperature, spectral band width, and similar lamp conditions. Nevertheless, it is highly recommended that one also use standard materials in the future. On the other hand, the m_o values provide a powerful quality control of the analytical procedure.

In flame AAS, the characteristic concentration $c_{1\%}$ depends heavily upon the nebulizer, its uptake rate (volume flow rate of the solution F_ℓ), and the distribution of droplet sizes in the aerosol. "It is always difficult with the flame AA to know how much analyte has been put into the optical path."[46,48]

This unfavorable situation has been improved by the introduction of the ionization suppression method for the determination of the dilution factor D_i. In the standardless flame AAS procedure for semiquantitative determinations,[41] the measurement of the calibration curve is replaced by the determination of the dilution factor D_i, which is then introduced into Equation 44 in order to get the experimental cluster G_{ex} of dimensionless factors. Finally, introducing G_{ex} into the simplified form of the sensitivity, the formula from Equation 26 gives the sensitivity S_A and the concentration c_A as $A(\lambda_o)/S_A$. Of course, the absorbance $A(\lambda_o)$ must be measured in the quasi-linear working range. This method will not be discussed in detail here, because it has an academic interest at the present time. Nevertheless, the possibility of absolute[48] or standardless[46] determinations by AAS is a fundamental aspect of AAS, and it could be of increasing interest in the future when the multielement AAS will be used more frequently for semiquantitative determinations, e.g., for the screening of waste waters.

E. Precision and Limits of Detection

The ability to detect a trace element or molecule in a given matrix is usually viewed in terms of the detection limit, which is the smallest concentration c_L (or quantity q_L) that can be derived from the smallest measure x_L and detected with reasonable certainty for a given procedure. In that sense, c_L (or q_L) is a combination of the precision of signal measurement and sensitivity S_c (or S_q):

$$c_L = ks_B/S_c \quad (\text{or } q_L = ks_B/S_q) \tag{45}$$

Problems[49] encountered in the comparisons of c_L (or q_L) values are the uses of different measures of the error and different statistical factors. According to IUPAC, the SD s_B of the blank measure x_B and a value of 3 should be used for k.

Nevertheless, detection limits based on statistical evaluation of the error of the concentration (or quantity) are more useful to the analytical chemist than limits based on measurements of the blank signal.

Very useful but seldom used measures of the concentration error (or quantity error) are the confidence limits (CL) of the concentration (or quantity) at a given confidence level,[50,51] e.g., at 95%:

$$CL(y_k) = (x_k - a)/b \pm ts(y_k) \tag{46}$$

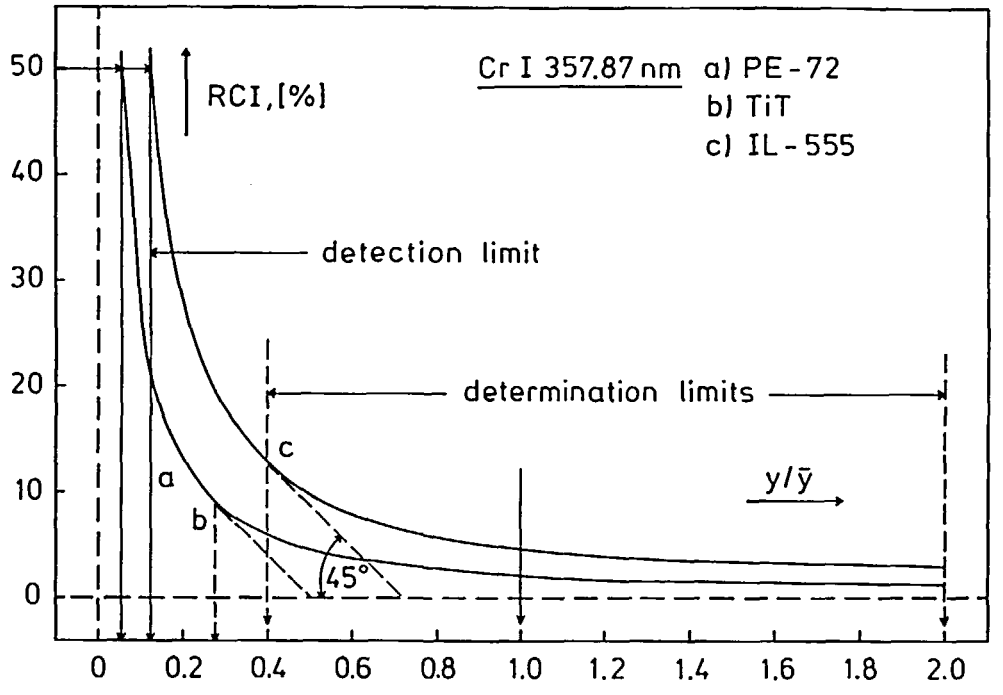

FIGURE 9. Dependence of the relative confidence interval RCI on the relative concentration or quantity ($y/\bar{y}$ = $c/\bar{c}$ or $q/\bar{q}$) (a) Conventional furnace AAS using a Perkin-Elmer 300 AA-spectrometer and a PE-72 furnace; (b) tube-in-tube technique[8] using the same instrument under the same experimental conditions as for (a) but with a small inner tube in the graphite tube of the PE-72 atomizer (see Figure 1); and (c) conventional furnace AAS using an Instrumentation Laboratory IL-751 AA-spectrometer and an IL-555 atomizer.

In this equation, x_k is the measure (absorbance $A[\lambda_o]$) from which the concentration c_k (or quantity q_k) is to be determined ($y_k = c_k$ or q_k). The intersept and the slope are a and b, respectively, of the regression line of x on y: $x = a + by$. The "student" distribution value at N-2 degrees of freedom and at the 95% confidence level is t. The number of the (x_i, y_i) pairs is N used for the determination of the analytical calibration function[52] $x = g(y)$ and $s(y_k)$ the estimated SD of the concentration (or quantity), for which most workers use the following approximate formula:

$$s(y_k) = (s_o/b)\left[\frac{1}{M} + \frac{1}{N} + \frac{(x_k - \bar{x})^2}{b^2\Sigma_i(y_i - \bar{y})^2}\right]^{1/2} \quad (47)$$

$$s_o = \left[\frac{\Sigma_i(x_i - (a + by_i))^2}{N - 2}\right]^{1/2} \quad (48)$$

The residual SD of the measure around the regression line of x on y is s_o, and M the number of measures taken for the determination of the concentration (or quantity) y_k in question.

As the absolute CL are very different in general, the relative confidence interval (RCI) (= 100ts $[y_k]/y_k$) will be used here for the graphical comparison of the performance of three different techniques of the graphite furnace AAS. RCI is a term easy to imagine because it simply is the "calculated analogue" of the well-known relative SD of the measure. The calibration curves a, b, and c (see Figure 9) were determined[9] by furnace AAS using a PE-72, IL-555-in-PE-72, and an IL-555 graphite tube, respectively (see Figure 1). The PE-300 and the IL-751 AA-Spectrometers were used for the determination of the analytical calibration

curves a, b (tube-in-tube technique, TiT), and c, respectively. Whereas M was set 2 for all three cases, the number of $(x_i,y_i) = A[\lambda]_i, q_{Cr,i})$ pairs were 15, 11, and 9 for the determination of the calibration curves a, b, and c, respectively. Also the time constants were different: 1/5 and 1/16 sec for the PE-300 (curves a, b) and IL-751 AA-Spectrometers (curve c), respectively. This may be the reason for the somewhat worse precision of the relative quantities $y/\bar{y}$ ($= c/\bar{c}$ or $q/\bar{q}$) obtained from the calibration curve c.

The determination limit $(y/\bar{y})_{max}$ at the upper concentration (or quantity) side is given by the requirement that all measures should be in the quasilinear working range, which is about two in maximum for a quasi-symmetrical distribution of the concentrations (or quantities) of the standard in the range of y: c_i or q_i. The determination limit[53] $(y/\bar{y})$ at the lower concentration side may be determined as the $y/\bar{y}$ value at the intersection point of the RCI curve and the straight lines drawn at 45° to the $y/\bar{y}$ axes. This procedure is similar to the procedure proposed[54] for the spectrographic methods of analysis: the determination limit is that amount of the component to be determined, at which the slope of a plot of the coefficient of variation vs. the amounts of the standard is -1. In general, the determination range should be limited to $0.5 < y/\bar{y} < 2$. The detection limit may be defined as the $y/\bar{y}$, at which the corresponding RCI value becomes 50%. These $y/\bar{y}$ values are 0.06 and 0.12 in the case of the calibration curves (a, b), and c, respectively. The lower plot in Figure 9 represents the RCI values for both calibration curves a and b, because the corresponding relative confidence intervals were practically the same. Multiplying the $(y/\bar{y})$ value by the corresponding means $\bar{q}$ of the Cr quantities q_i atomized (592, 102, and 80 pg on the average), one obtains the detection limits of 36, 6, and 10 pg for the performances a, b, and c, respectively.

As the graphic representation of the precision is not suitable for routine work, the use of $RCI(\bar{y})$ at the concentration (or quantity) mean $\bar{c}$ (or $\bar{q}$) is recommended. At this point x_k is equal to $\bar{x}$ and therefore the RCI-term simplifies to (see Equation 47):

$$RCI = 100t(s_o/b\bar{y})\left[\frac{1}{M} + \frac{1}{N}\right]^{1/2} \tag{49}$$

$RCI(\bar{y})$ amounted to 5.6, 4.9, and 5.4% in the cases a, b, and c, respectively.

It would be very valuable for comparisons, if the analyst would report three different measures of the quality of analytical performance:

1. $3s_B/S$, which is a measure of the instrumental performance
2. $3s_o/S$, which is a measure of the instrumental and methodical performance
3. $RCI(\bar{y})$ as a measure of the precision of determinations in the middle of the linear working range

As $3s_o/S$ and $RCI(\bar{y})$ are obtained as "byproducts" of the calibration, only a few and simple additional calculations must be carried out. Value $3s_B/S$ may considerably deviate from the ideal values c_L^{id} (or q_L^{id}) published by manufacturers for their instruments and by researchers for proposed new analytical techniques. These detection limits are usually obtained under ideal conditions with highly optimized parameters. Under practical laboratory conditions, it may not be possible to approach these quoted detection limits by closer than a factor[55] 5 or 10. Furthermore, the methodical component of $3s_o/S$ may be markedly higher than $3s_B/S$, resulting in an even larger ratio ($[3s_o/S]/c_L^{id}$ or q_L^{id}) than 10. Indeed, a detection limit c_L^{id} of 4 ng/L Cr is given in the "Guide to Analytical Values for IL Spectrometers, 1982."[56] This value is valid for a 100 µL dosage, and therefore it corresponds to an absolute detection limit q_L^{id} of 0.4 pg or to a ratio ($[3s_o/S]/q_L^{id}$) of 18 ($= 7/0.4$).[9] The use of the residual SD s_o for the calculation of $RCI(\bar{y})$ is correct. Nevertheless, the SD of the absorbances increase

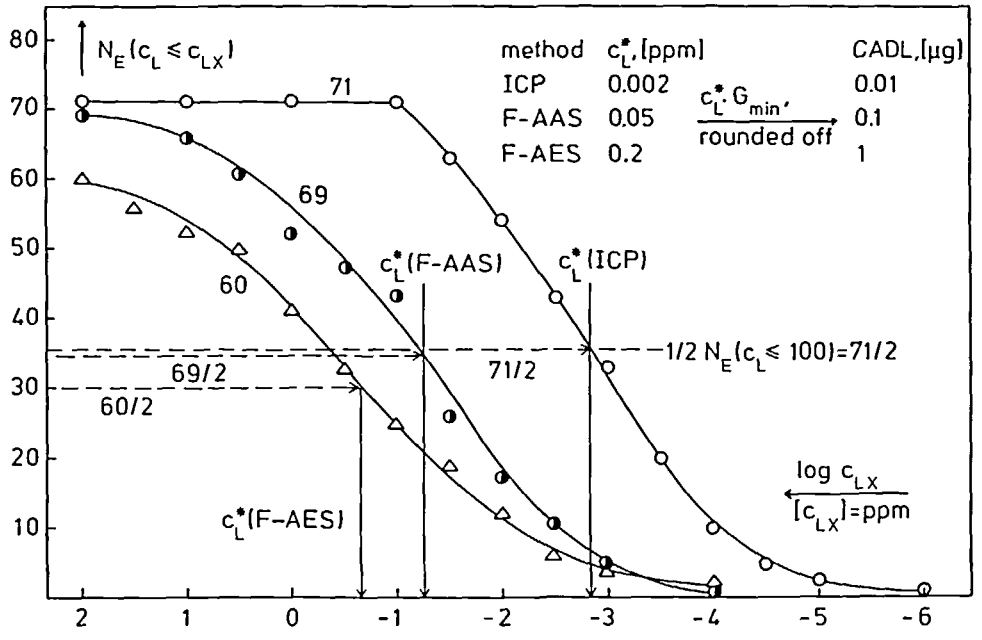

FIGURE 10. Estimation of characteristic detection limits c_L^* and characteristic absolute detection limits (CADL) for the three atomic spectrometric methods: atomic emission spectrometry using an inductively coupled argon plasma (ICP) as atom reservoir, flame atomic absorption spectrometry (F-AAS), and flame atomic emission spectrometry (F-AES). c_{LX} is the preselected detection limit, N_E the number of elements with a c_L-value equal to or smaller than c_{LX}. The minimal sample amount, G_{min}, needed for a good reading of the measuring signal, was set to 5 g here.

linearly with the increasing absorbances. Therefore, $3s_o/S$ gives a rather overestimated limit of detection. A more precise procedure would consist in the use of weighted regression lines.[51] Although weighted regression calculations are more complicated to perform than their unweighted counterparts, they give much more realistic results for the confidence limits of predicted concentrations. Therefore, the use of weighted methods should be encouraged.

Although the analytical relevance of the c_L^{id} (or q_L^{id}) is questionable, these ideal values are very useful for comparison of different methods and techniques. In order to obtain a characteristic c_L^* value for a given technique,[57] the number N_E of elements, which have c_L^{id} values smaller than or equal to a chosen value, e.g., 100, 10, . . . , 0.01, 0.001, etc. µg/g (≅ppm) was plotted against a chosen $\log(c_L^{id})$ value. The c_L^{id} value, at which the initial number of elements is lowered to the half, was taken as the characteristic detection limit c_L^* of the method in question (see Figure 10).[6b] The c_L^* value may be converted to the characteristic absolute detection limit (CADL) by multiplication with G_{min}, which is the minimal sample amount to be taken for a good reading of the measuring signal.

Alternatively, the methodical characteristic mass $q^*_{1\%}$ may be used for comparison of the methods. This is also obtained graphically from curves "N_E vs. $q_{1\%}$". The mass yielding 1% absorption is $q_{1\%}$ (or 0.0044 absorbance units): $q_{1\%} = 0.0044/S_q$. In order to obtain the methodical characteristic mass for a given method (see Figure 11), the number N_E of elements, which have $q_{1\%}$ values smaller or equal to a chosen value, e.g., 10^{-5}, 10^{-7}, . . . , 10^{-13} g/% was plotted against the chosen $\log(q_{1\%})$ value. The $q_{1\%}^*$ value, at which the initial of N_E is lowered to the half, may be considered as a characteristic of the method in question. The $q_{1\%}^*$ values of 10^{-6} and $10^{-11.3}$ g/% were obtained for flame and furnace AAS, respectively, using the data for Instrumentation Laboratory AA-Spectrometers.[56] The markedly better value of $10^{-11.8}$ g/% was obtained for the L'vov furnace.[10,38] The higher

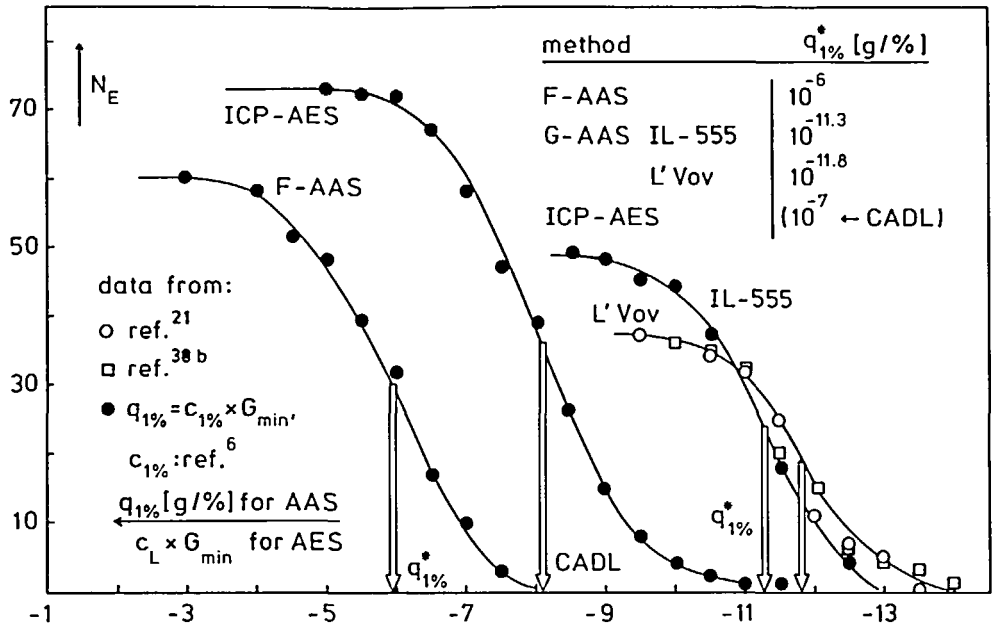

FIGURE 11. Estimation of methodical characteristic masses $q^*_{1\%}$ for flame atomic absorption spectrometry (F-AAS), atomic emission spectrometry using an inductively coupled argon plasma as atom reservoir (ICP-AES) and graphite furnace atomic absorption spectrometry (G-AAS) using the L'vov atomizer and the Instrumentation Laboratory IL-555 atomizer, respectively. For ICP-AES the absolute detection limits were used, which were calculated from the corresponding characteristic concentrations $c_{1\%}$, taken from the compilations in the appendixes of Reference 6: $q_{1\%} = c_{1\%} \times G_{min}$, whereby 5 g solution were considered to be the minimal quantity, G_{min}, needed for the determination of the SD s_b of the blank measure ($q^*_{1\%}$ was set equal to 10 × CADL as an empirical rule of thumb).

sensitivity of the last atomizer is a consequence of the smaller inner radius of the graphite tube of the L'vov atomizer. The ratio of the squares r_i^2(IL)/r_i^2(L'vov) is $(\frac{4.5}{2})^2/(\frac{2.5}{2})^2 = 3.2$, which is the same as the enhancement factor $10^{-11.3}/10^{-11.8}$ in excellent agreement with the prediction of Equation 4.

F. Accuracy of Determinations of Main Elements by Flame AAS

The accuracy of the results obtained by AAS depends on the quality of calibration. Possible systematic errors should be eliminated as completely as possible.

1. Spectral interferences can generally be eliminated by use of small spectral band-widths of the monochromator. Thereby, the bending of the calibration curves is also reduced[58,59] in general, but it cannot be eliminated completely because stray light always causes some bending.[60,61]
2. In order to eliminate chemical interferences, the temperature and number density of oxygen must be so high and small, respectively, that dissociation of the most stable compounds (mostly monoxides) becomes as complete as possible (see Introduction). The use of strongly reducing flames and releasers, e.g., La(III) for the releasing of other metals from phosphates or pyrophosphates, are additional helps at flame temperatures. Matrix modification is especially important in furnace AAS.
3. Ionization interferences are easily eliminated by addition of ionization buffers to increase the concentration of free electrons in the flame gases, thus repressing and stabilizing the degree of ionization.

4. Physical or nonelement specific interferences affect the amount of sample passing through the measuring beam of the source. They include the volume flow rate F_ℓ of the solution, the efficiency of nebulization ϵ_n. As F_ℓ and ϵ_n are dependent on the viscosity and surface tension of the solution, the temperature of standard and analysis solutions must be the same. The physical properties of the solutions are also dependent on the concentration of main components, thus they must be matched in standard and analysis solution to about 10% (rel.). Otherwise, the analyte addition method or standard addition method must be used. Although this method is an extremely valuable tool, several conditions must be met for obtaining accurate results:[55]

- The analytical curve must be linear.
- The added standard must be in the same chemical form (oxidation state, complexion).
- *Multiplicative interferences must be constant over the concentration range of the samples* and addition standards.
- Additive interferences must be absent or corrected for.

The determination of the main elements of new compounds challenge the highest requirements of accuracy to analytical results. In the 1970s, AAS was used to prove the substance formula for 430 new complexes containing 20 different transition metals and alkali metals as counter ions of complex anions. All 430 solid samples were analyzed by the analytical group of the author according to the following standard procedure:

1. In order to check for possible inhomogenity of the sample in question, always two independently weigh-in quantities were analyzed.
2. The samples were dissolved either in 0.1 *M* HNO_3 or in dimethylformamide. Some complexes of the platinium group metals were dissolved in 1 *M* HCl in order to stabilize the solutions by formation of chlorocomplexes. Insoluble complexes were oxidized by HNO_3 at 550 to 600 K in sealed pyrex glass tubes. (10%[v/v] HCl was added in the case of platinium group metals.) The oxidized samples were diluted with water to get a HNO_3 concentration of 0.1 ($\pm$ 10%) *M*. One part of each solution was further diluted with 0.1 HNO_3 (or 1 *M* HCl in the case of platinium group metals). The dilution factors were selected in such a way that the absorbances were distributed in the range $0.5 < A(\lambda_o)/\overline{A}(\lambda_o) < 2$ of the relative absorbances. The average of absorbances measured for the five standard solutions is $\overline{A}(\lambda_o)$.
3. All five standard and four analysis solutions were atomized twice in the suitable air/acetylene or N_2O/C_2H_2 flame, whereby the measuring order of solutions was symmetrically reversed. By this precaution, small systematic errors are compensated, which might have been caused by a small quasilinear change of the sensitivity during the analysis time.
4. The analytical evaluation function $c = f(x)$ was represented by a linear or parabolic regression line, respectively, depending on the curvature of f(x). In general, the linear regression line was calculated first. If the square r^2 of the correlation coefficient was smaller than 0.995, a parabolic regression line was preferred for $c = f(x)$. From the eight percentages (%A) obtained for the same sample, the average $(\%A)_{av}$ and its CL at the 95% confidence level were calculated.

$$\text{Result: } (\%A)_{av} \pm ts(\%A)(N)^{-1/2}$$

$$N \geq 8 \qquad (50)$$

the t-distribution value at N-1 degrees of freedom and at the 95% confidence level is t, and s(%A) is the SD of (%A).

5. The analysis was considered as finished if the relative confidence interval (RCI) = $100\ ts(\%A)(N)^{-1/2}(\%A)_{av}^{-1}$ was smaller or equal to 2% and the relative deviation from the theoretical value RDT was also smaller or equal to 2%.

$$\text{Criterion I: RCI} \leq 2\%$$

$$100|(\%A)_{AAS} - (\%A)_{th}|/(\%A)_{th} = \text{RDT} \leq 2\% \quad (51)$$

6. If the precision was insufficient (RCI > 2%), but no systematic error was indicated by RDT (<2%), the number N of absorbance measurements was enhanced so far as the relative confidence interval RCI became smaller or equal to 2%.
7. If RDT was greater than 2%, the analysis was repeated using a control method CM, mostly X-ray fluorescence spectrometry, XRF, molecular absorption spectrometry (MAS), and AES using an inductively coupled argon plasma as atomizer, ICP-AES, respectively. In the case of

$$\text{Criterion II: } 100|(\%A)_{AAS} - (\%A)_{CM}|/(\%A)_{CM} = \text{RDC} \leq 2\sqrt{2} \quad (52)$$

it was concluded that the substance formula assumed for the new complex compound was not correct. RDC is the relative deviation from the control result.

8. In a few cases, the experimental values $(\%A)_{AAS}$ and $(\%A)_{CM}$ obtained by AAS and the control method CM, respectively, were not the same within their allowed deviation of $2\sqrt{2}\%$. In such cases, analytical methods have been controlled by a third method.

From the total 770 determinations of main elements of the 430 compounds mentioned above, 710 results fulfilled the criterion I (see Equation 51). In 45 cases of the total 60 undesired results, the criterion II for the absence of a systematic error was fulfilled, i.e., the proposed substance formula was incorrect. In the remaining 15 cases, systematic errors in the $(\%A)_{AAS}$ were detected. These errors were caused by chemical interferences. No such interferences were detected for ICP-AES.

G. Conclusions

The best analytical method has the best selectivity and precision coupled with high sensitivity, permitting the determination of a large number of species. The instrument required should be cheap to buy and easy and inexpensive to operate. Such an ideal method does not exist, but AAS has characteristics pointing in this direction.[6] Nevertheless, flame AAS will be partly replaced by ICP-AES in the near future. The advantages of the last method are: (1) very fast multielement analysis, (2) about ten times better relative sensitivity as measured by the characteristic detection limit c_L^* (see Figure 10), (3) linear working range in five orders of magnitude, (4) practically no chemical and ionization interferences, because the ideal conditions $0.99 < \beta_a < 1$ and $(\gamma)_a/(\gamma)_s = 1$ can be much better realized using ICP than flames, and (5) no spectral sources are needed.

On the other hand, furnace AAS has about 10^4 times a better absolute sensitivity as measured by the methodical characteristic mass $q_{1\%}^*$ (see Figure 11) than ICP-AES. Furthermore, AAS provides a much better selectivity at much lower costs than ICP-AES. Therefore, furnace AAS cannot be superseded by ICP-AES in the trace analysis of complex samples, which is one of the most growing fields of chemical analysis.

The analytical approach ICP-AAS shows as high a selectivity and precision as flame AAS. These features indicate its use for the determination of metals in complex compounds, which are difficult to dissociate into atoms in flames. Nevertheless, ICP-AAS will not be a frequently used method because of its low sensitivity. On the other hand, the atomic fluorescence spectrometry using ICP as atom reservoir combines the advantages of flame AAS concerning selectivity and those of ICP-AES concerning sensitivity and freedom of

chemical and ionization interferences. Therefore, the analytical approach ICP-AFS might receive more attention in the future.

III. FUNDAMENTAL ASPECTS OF INSTRUMENTATION AND METHODOLOGY

A. Background Correction

The compensation of nonspecific background absorption is the main problem connected with determinations of traces of metals in the presence of large amounts of concomitants that volatilize together with the metal to be determined. This analytical problem manifests itself especially in the graphite furnace AAS used in trace analysis of complex samples and in coordination chemistry.[62] Scattering of the incident radiation by solid or liquid particles in the atom reservoir and also the absorption by molecular species cause absorption signals that generally exhibit broadband character: $\delta\lambda_m > \Delta\lambda_m \gg \delta\lambda_a$, where $\delta\lambda_m$ and $\delta\lambda_a$ are the half-intensity widths of the molecular absorption band and the atomic absorption line, respectively, and $\Delta\lambda_m$ is the spectral band width of the monochromator. If the diameter 2r of the scattering particles is small, compared with the wavelength, e.g., $2r \lesssim \lambda/10$, the relative scattered intensity I_R/I_o is proportional to the number of density n_p of scattering particles divided by the fourth power of the wavelength: $I_R/I_o = k_R n_p \lambda^{-4}$ (Rayleigh's scattering law). According to this law, the compensation of background absorption, due to scattering, is especially important in the UV-range.

The background correction methods, which have been developed for AAS, consist either in recording of the atomic absorption profile of the resonance line λ_o using a tunable dye laser[63] or a high resolution Echelle monochromator[64] or in the use of two beams passing the atom reservoir, the measuring and reference beam, respectively, which have different absorption characteristics and are time resolved. Figure 12 shows the development of the reference beam methods:

1. The two line correction method[65] utilizes the comparison of the intensity $I(\lambda_o)$ of the resonance line with the intensity $I(\lambda_r)$ of a reference line λ_r, emitted by the analysis element, an accompanying element in the hollow cathode or by atoms of the filling-gas of the HCL. The separation of λ_o and λ_r should be as small as possible, but a mixing of the intensities $I(\lambda_o)$ and $I(\lambda_r)$ by the monochromator must not occur: $|\lambda_r - \lambda_o| \geq \Delta\lambda_m$ (see line profiles a in Figure 12).
2. For the polychromatic beam method[66] the intensity $I(\lambda_o)$ is compared with the intensity $I_\lambda \Delta\lambda_m$ of the polychromatic source (Deuterium arc or a filament lamp) falling into the spectral band widths $\Delta\lambda_m$ of the monochromator. It should be noted that the polychromatic beam was already used[67] for background correction in the analysis of Hg in 1954.
3. For the self-reversal method,[68] the same resonance line λ_o is generated in different experimenatl conditions providing a sharp line for the measuring beam and a strongly broadened line due to pressure broadening and self-reversal for the reference beam, which is practically not further absorbed by the atoms of the analysis element.
4. For the direct Zeeman Effect Atomic Absorption or Emission Zeeman Effect Atomic Absorption (EZ-AAS) the intensities I_π and $I_{\sigma\pm}$ of the Zeeman components λ_π and $\lambda_{\sigma\pm}$ of the resonance line λ_o, emitted in an external magnetic field, are compared.[69] Only the π component is absorbed by atoms: $\lambda_\pi = \lambda_o$.
5. For the inverse Zeeman Effect Atomic Absorption or Absorption Zeeman Effect Atomic Absorption (AZ-AAS) the intensities I_π and $I_{\sigma\pm}$ are compared.[70] Again, only the π component is absorbed by the atoms of the analyte because the $\sigma\pm$ absorption profiles are shifted from the position $\lambda_o = \lambda_\pi \neq \lambda_{\sigma\pm}$.
6. The Smith-Hieftje system is a special self-reversal method using the same HCL for the generation of a narrow line and a strongly self-absorbed line, respectively.[71]

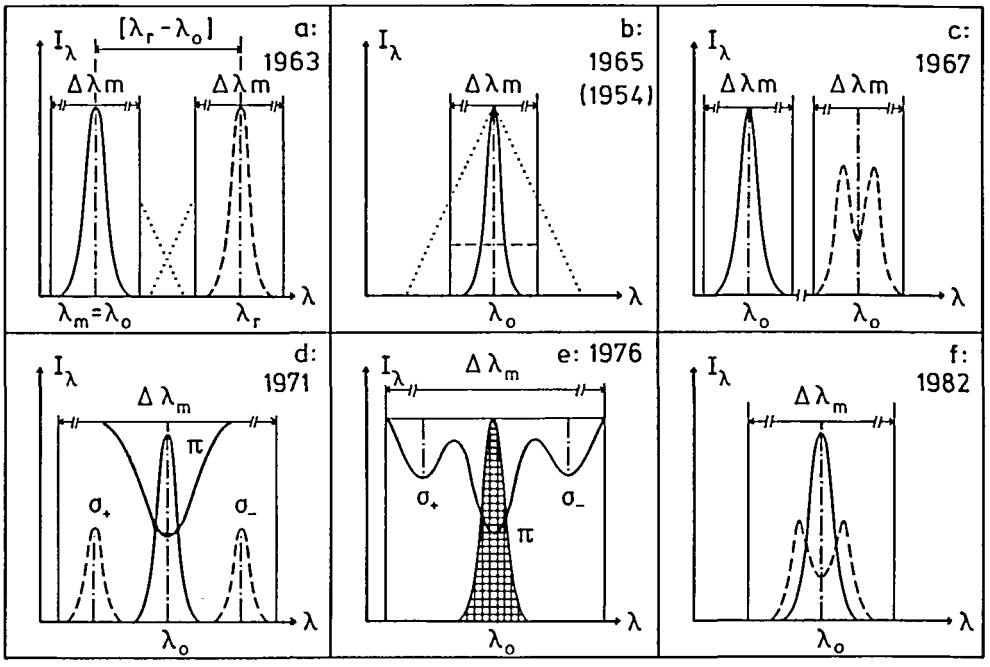

FIGURE 12. Diagrams for comparison of the background corrections (BC) using different reference beams: (a) two-line BC, (b) deuterium BC, (c) self-reversal BC, using two different sources, (d) direct or emission Zeeman effect BC, (e) inverse or absorption Zeeman effect BC, and (f) Smith-Hieftje BC (self-reversal BC using one source). The profiles of the emission lines are represented by the relative spectral intensity I_λ, which is drawn as a solid line and a dashed line for the measuring and reference beam, respectively. Both emission profiles are the same in the ideal case of (e). The absorption profiles in diagrams (d) and (e) are thought to be copied by absorption of polychromatic radiation, which has a constant relative spectral intensity in the narrow spectral range of $\lambda_o \pm \Delta\lambda_m$ where $\Delta\lambda_m$ is the spectral band widths of the monochromator. Dotted lines in Figures (a) and (b) indicate the instrumental broadening. A small collisional shift of the absorption line profile in respect to the source line profile was neglected in Figures (d) and (e).

If the absorption profiles are recorded, the compensation power is dependent upon the resolution: the more resolving power, the better the background correction. For the compensation of the background, by comparison of the intensities of the measuring "m" and reference "r" beams, the following requirements should be fulfilled (index "o" means before the atomizer):

1. The reference beam should not, or as slightly as possible, be absorbed by the atoms of the analyte: $(I_r^o - I_r)/I_r^o \rightarrow 0$.
2. The measuring and reference beam should be attenuated by scattering and molecular absorption to the same degree: $I_m/I_m^o = I_r/I_r^o$.
3. The time resolution of the background correction system, which is the time t_{mr} between the measurements of I_m and I_r should be so small that the background correction is accomplished correctly even at rapid changes of the number densities of the analyte, molecules, and solid or liquid particles (t_{mr} of 10 msec or less are suitable for volatile elements).

The first requirement (see above) is completely fulfilled by the first method and almost completely by the second method: $S_A^{DL} \simeq S_A(1 - \delta\lambda_a/\Delta\lambda_m)$ (see Equation 25). The sensitivities obtained with and without a deuterium lamp (DL) as background corrector are S_A^{DL}

and S_A. The ratio of the half-intensity width $\delta\lambda_a$ and the spectral band width $\Delta\lambda_m$, used for both determinations, varies from line to line and depends on the $\Delta\lambda_m$ needed for the separation of the resonance line λ_o. $\delta\lambda_a/\Delta\lambda_m$ Is of the order of 0.01. How well the first requirement is fulfilled in methods, three, four, five, and six, respectively, depends upon the magnetic flux density B received by the emitting or absorbing atoms and upon the degree of self-reversal, respectively.

The ratio of the sensitivities measured by Zeeman Effect AAS (index ZE) and AAS without background correction (index A) may be estimated[62] by

$$S_{ZE}/S_A = \frac{(b/D)_{ZE}}{(b/D)_A}(1 - R) \tag{53}$$

The construction factors (see Section II.A) are the same if the same atomizer is used for both techniques, e.g., if a Zeeman system using an alternate current (ac) electromagnet is working in the Zeeman mode (electromagnet on) and in the conventional mode (electromagnet out), respectively. In comparison of different systems, the ratio of the construction factors may be markedly different in general, e.g., in the case of a Hitachi 170-70 Zeeman effect atomic absorption spectrometer and a Perkin Elmer PE-300 AA spectrometer $(b/D)_{ZE}/(b/D)_A$ was[62] 2.0.

R is the fractional reduction in sensitivity.[72] It depends on the magnetic flux density B and the Zeeman pattern of the line in question. Furthermore, R depends also on the Zeeman system used, i.e., whether B is generated by an alternate or direct current or even if it originates from a permanent magnet. At a frequently used B value of 1 T (= 10^4 G) the fractional reduction of sensitivity is in the range of 0.05 to 0.4. High R values are expected for elements having an anomalous Zeeman pattern and hyperfine structure due to isotope shift or/and to coupling of the magnetic moments of electrons and the nucleus. Fortunately, it has been found that elements having many isotopes, such as Hg and Pb, do not pose any problem with overlapping between the π and $\sigma\pm$ components due to hyperfine structure when a magnetic flux density of 1 T or more is applied.[73] The ratio $(c_L)_{ZE}/(c_L)_A$ of the detection limits were determined[73] for 19 elements using a permanent magnet at 1.1 T and a conventional AAS with a similar type of graphite furnace. Eighteen values are between 0.5 and 4 obtained for the Co 240.7 nm and the Al 309.2 nm line, respectively. These give an average value of 1.50 ± 0.47. As the deviation of the average value from one does not markedly exceed its confidence limit at 95% confidence level, it may be stated that the AZ-AAS and the conventional furnace AAS have about the same detection power. It is interesting to note that the Co 240.7 nm line arises from the transition $^4F_{9/2} - {}^4G_{11/2}$. As each energy level is split into (2J + 1) Zeeman levels, a very complicated Zeeman pattern occurs, and the sensitivity decrease is especially high. Despite this fact, a better detection limit was obtained for the inverse Zeeman AAS than for the convential AAS. Apparently, the excellent stability of the intensity ratio $I_m/I_r = I_\pi/I_{\sigma\pm}$ makes this improvement of the detection limit possible despite a decreased sensitivity.

It should be stressed that there are minor practical and fundamental differences between different Zeeman systems. de Galan and de Loos-Vollebregt[74] have drawn the following important conclusions from theoretical considerations:

1. A constant transversal magnetic field in conjunction with a rotating polarizer may be simpler and cheaper to obtain, but it has the disadvantage of reduced sensitivity and a more pronounced nonlinearity in the quite common case of the anomalous Zeeman effect.
2. A transversal variable magnetic field in conjunction with a polarizer or especially a longitudinal variable magnetic field are preferred. In this latter case no polarizer is needed, and therefore no light loss, due to it, occurs.

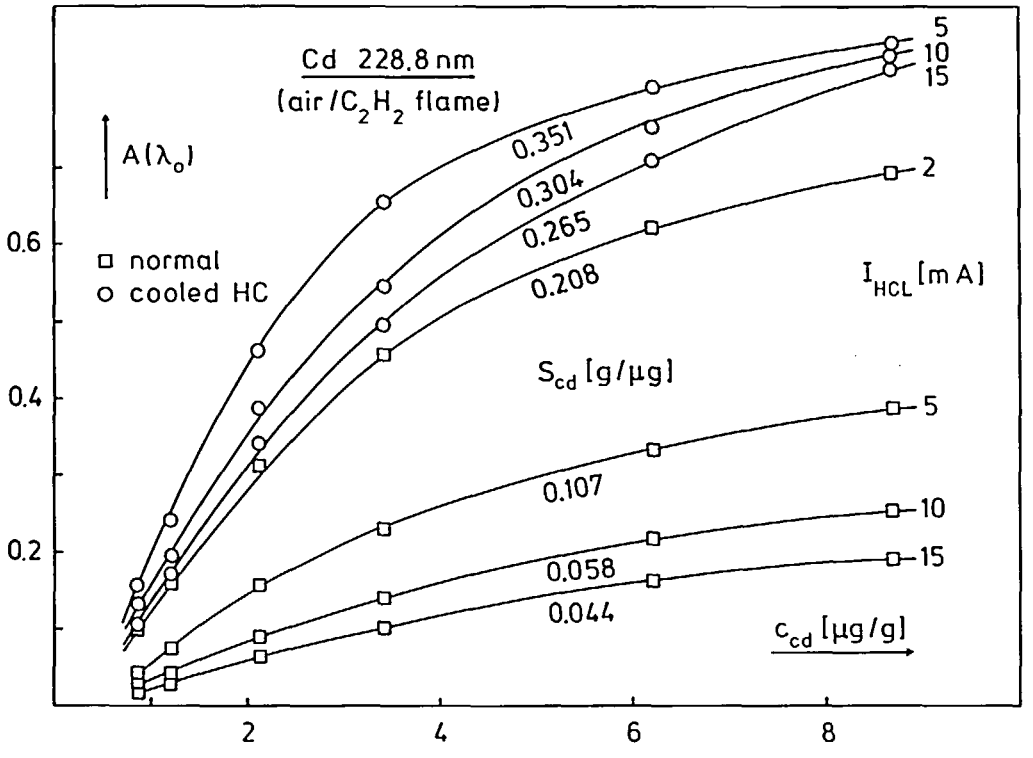

FIGURE 13. Dependence of the sensitivity S_{cd} on the kind of the hollow cathode and the lamp current I_{HCL}. The upper three calibration curves were obtained with a homemade[5] demountable hollow cathode lamp (HCL). The bulk material of the cathode was cooled by blowing through air at room temperature. The other calibration curves were taken by using an Instrumentation Laboratory Cd-HCL in the normal mode at different I_{HCL}.

Requirement 1 is better fulfilled the higher the degree of self-reversal produced by the Smith-Hieftje background correction technique is. For a figure-of-merit to indicate line broadening, a parameter termed "modulation depth" was defined[75] as the ratio of the slopes of working curves obtained with the Smith-Hieftje background correction method and with conventional low-current operation. During this 9-msec low-current pulse, the resonance line λ_o is emitted without self-reversal and therefore is effectively absorbed by the analyte atoms. In the following 0.3-msec high-current pulse, a strongly broadened reference line is emitted, which is much less absorbed by the analyte atoms. The dependence of the sensitivity on the lamp current is especially strong in the case of volatile elements, e.g., Cd (see Figure 13). It must be stressed for clarity, that these curves were obtained not by the Smith-Hieftje method but by using a conventional double channel AA-spectrometer (Instrumentation Laboratory IL-751). Using two HCLs for the same element in the channels A and B at strongly different lamp currents I_{HCL}, the principle of the background correction by self-reversal of the resonance line can be impressively demonstrated. For that purpose the absorbances $A(\lambda_o)$ obtained for solutions containing 4 ng Cd/g, 0.1 *M* HCL, and NaCl at different concentrations were measured using two conventional Cd-HCL fed by 2 and 10 mA, respectively (see curves a and b in Figure 14). The absorbance measured in channel A became 1.85, which is the highest absorbance accepted by the instrument used (IL-751). Therefore, solutions containing more NaCl could not be measured. The difference of the absorbances measured in channel A and B is the atomic absorption of Cd. The average value of 0.300 ± 0.040 (SD) is apparently smaller than the average value of 0.531 ± 0.36 SD obtained by the DL correction method having a fractional reduction $R_{DL} \lesssim 0.01$. The modulation depth MD can easily be calculated according to its definition given above:

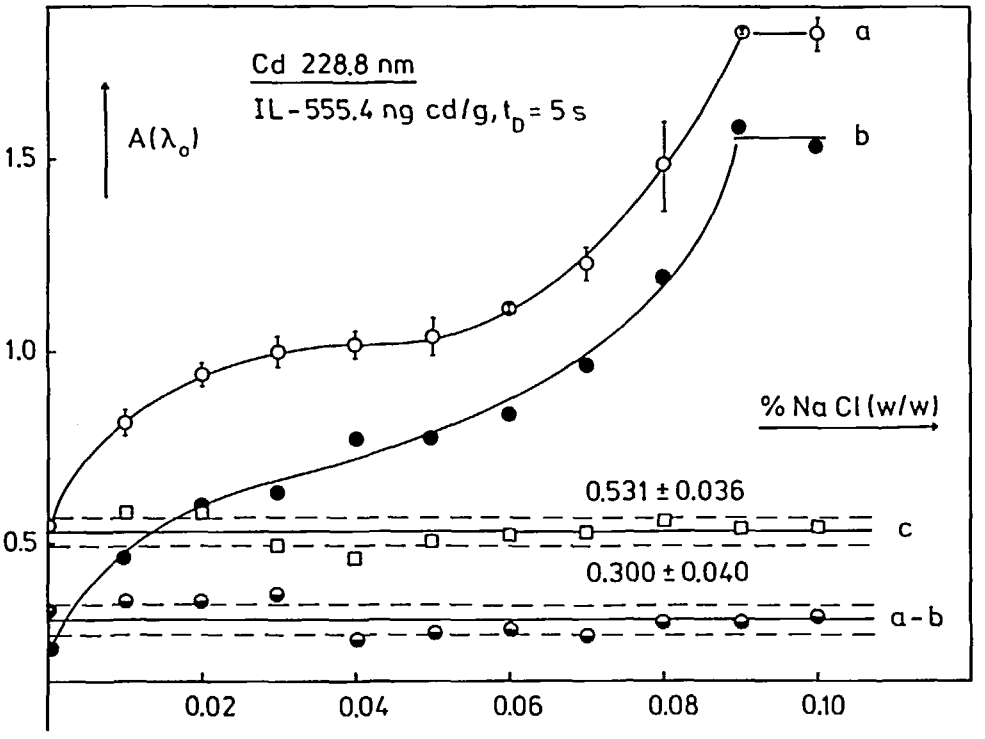

FIGURE 14. Demonstration of the working principle of the background correction (BC) by self-reversal using two sources. An Instrumentation Laboratory IL-751 AA-spectrometer was operated with two Cd-HCLs from the same instrument maker. The HCLs in the channels A and B were operated with 2 and 10 mA, respectively. The difference a-b of the absorbances measured at 2 and 10mA, respectively, is the background corrected atomic absorption. In order to enhance the background absorption, Cd solutions containing 4 ng Cd/g and increasing concentrations of NaCl were introduced into the graphite tube using the IL-FASTAC aerosol introduction system. The deposit time t_D was 5 sec. The background corrected absorbances (c) were obtained by a deuterium BC.

$$MD = S_{SH}/S_A = (S_{lc} - S_{hc})/S_{lc} = 1 - R_{SH} \quad (54)$$

S_{lc} and S_{hc} are the sensitivities measured at low and high lamp current, respectively. As R_{DL} may be considered as vanishingly small for the deuterium background correction, MD is simply obtained as the ratio of the average values given above: 0.57 or 57%. Setting the highest (0.351 g/μg) and the lowest (0.044 g/μg) value from Figure 13 for the sensitivities S_{lc} and S_{hc}, respectively, one obtains a modulation depth of 87% for the self-reversal method using two Cd-HCLs at strongly different conditions.

The mean modulation depth obtained for the SH-correction method[75] was found to be 53% with a SD of 21%. Over all, the modulation depths ranged from a low of 16% (Hg) to a high of 87% (Cd). Using the average value of $\bar{R}_{ZE} = 0.18 \pm 0.13$ SD calculated from the 19 R values given in Reference 72 for a magnetic flux density B of 0.9 T, a mean "modulation depth" for the inverse Zeeman effect background correction is obtained as $(1 - \bar{R}_{ZE})$. The resulting value of 0.82 is markedly better than the mean modulation depth of the Smith-Hieftje method. The requirement 2 for an accurate background correction by the reference beam methods a to f is all the better fulfilled the more the following idealized conditions can be realized:

2.1 — The wavelengths λ_m and λ_r of the measuring and reference beams at the maxima of the corresponding line profiles should be the same. This is almost completely fulfilled by the method 5 (a small collisional shift of the absorption profile was neglected in Figure 12e). In the case of the polychromatic reference beam method 2, the equivalent of λ_m and

λ_r does not arise from the physical nature of the beams but from the fact that the central wavelengths must be equated by correct adjustment of the monochromator. The difference $|\lambda_m - \lambda_r|$ is very small, e.g., 2 to 5 pm, for the direct Zeeman effect background corrections, and it is even markedly smaller in the case of the self-reversal methods 3 and 5. In general, these differences may be completely neglected for the discussion of broadband molecular absorption and scattering by solid or liquid particles. Line pairs[76] with $|\lambda_m - \lambda_r|$ values between 0.1 and 8.5 nm have been reported in the case of the two-line background correction method 1. Because the absorption signal from the Rayleigh scatter increases with the fourth power of the reciprocal wavelength, the background correction error may become substantial at short wavelengths if the line chosen is more than 1 nm apart from the analyte line.

2.2 — The optical alignment of the measuring and reference beam should be the same. This is automatically achieved by the reference beam methods using the same spectral source for both beams: 4, 5, and 6. Single channel instruments with continuum source for background correction 2 are, however, probably the most difficult to set up.[76] Not only does the atomic spectral source need to be aligned optically with the continuum source, but usually, their power outputs also have to be matched. This is done by attenuating one beam or changing source power by adjusting the current. The adjusting of slit width would be a very powerful method for the matching of the powers of a monochromatic and continuum source because the relative intensities I_m and I_r increase linearly and quadratically, respectively, with the spectral band width $\Delta\lambda_m$ of the monochromator. But this is generally not recommended in the case of the transition metals because the radiances of the resonance line and weakly absorbed or unabsorbed lines are mixed at greater $\Delta\lambda_m$ values resulting in decrease of the sensitivity.[58,59] In single channel double beam systems the intensities I_m and I_r for both sources can be measured and rationed. The power input of the reference source can be varied automatically in order to match the power outputs of the sources. Automatic gain control circuitry can be used to set the photomultiplier dynode voltages in accordance with the intensity of the reference beams. The requirements for alignment of the sources of double channel instruments are not very different from those of double beam single channel instruments.

2.3 — In order to correct a strong wavelength-dependent background, the relative spectral intensities $I_{\lambda m}$ and $I_{\lambda r}$ or the line profiles should also be the same. This requirement is almost completely fulfilled only by the inverse or absorption Zeeman effect background correction 5. At a glance to Figure 12, the "quality order" of the methods with respect to the requirement 2.3 will obviously be e > f (= c) > d > a > b. The best fulfilling of this requirement by method 5 is clearly demonstrated by the fact that this background correction is not affected by spectral interferences due to the OH radical in analysis of Bi, whereas method 4 shows an OH effect.[73] Theoretically, the background may depend on the magnetic flux density B, but this dependence does not reveal itself virtually by experiments because of the weak coupling of molecular magnetic moments with an external magnetic field.

Method 3 is limited to Hg and some volatile metals, e.g., Cd (see Figure 14). Furthermore, practically all conventional AA-spectrometers are provided with a deuterium arc background corrector (DL). Therefore, the last part of this section is limited to the discussion of methods 2, 4, 5, and 6.

A deuterium arc built-in into an AA-spectrometer with optimized optical and electronic system produces a very good correction of unstructured background. An accuracy of ± 0.02 absorbance units (AU) has been reported[77] at a background level of 2.0 AU. This may be the best value achieved by method 2. Nevertheless, incorrect results may be obtained for molecular absorption due to vibration transitions, because the DL averages the background across the spectral band width $\Delta\lambda_m$ of the monochromator resulting in an under- or over-compensation for a greater or smaller average than the effective background at the central wavelength λ_o, respectively.

For complex matrixes, such as blood serum, urine, fishmeal, seawater, sludge, etc. structured backgrounds are likely to arise in the atomization step of the furnace AAS. In such cases, e.g., the determination of Pb in serum at the 283.3 nm line, the Zeeman effect background correction 5, resulted in an accuracy of 0.005 AU at 2 AU background level: this was at least a factor five better than the correction obtained from the DL-corrector even after careful alignment.[72] The Zeeman effect techniques have received independent examination from several groups of workers under some extremely testing experimental conditions. From the data thus obtained, it is evident that the background correction efficiency of the method is very significantly superior to that of the continuum background correction systems.[78]

The seven configurations[73] of Zeeman effect atomic absorption (ZAA) and the Smith-Hieftje (SH) background corrections system have the common feature that they are using the resonance line of a single spectral source for the measuring and reference beam. Therefore, the requirements 2.1 and 2.2 are automatically fulfilled. The very important consequences are:

1. Background correction can be affected in the visible as well as in the UV region of the spectrum.
2. The optical system is impossible to misalign because it has identical geometry for both beams. Therefore, very high backgrounds can be corrected. Furthermore, the source noise is eliminated by these real double beam systems.
3. Accurate correction for structured background can be made.
4. Correction of spectral interferences is possible.[79] This possibility is scientifically interesting but has no great analytical significance.[80]

Concerning the advantages 3 and 4 over the DL-background correction, the different ZAA configurations and SH systems show some differences in the background correction efficiency (see 2.3). The latter mentioned system has some advantages and disadvantages over ZAA:[81]

1. No double-valued working curves ("rollover") are obtained with the SH system.[81] This statement seems not to be true at higher concentrations, but it remains true that quantitatively the phenomenon is less severe than in the Zeeman system.[82]
2. The SH system is more light-efficient than ZAA because no light loss occurs due to the polarizer.
3. The SH system can easily be applied in combination with any atomizer, e.g., furnace or flames because it does not constrict the sample areas. Of course, this is also true for the direct ZAA but not for the inverse ZAA.
4. The SH system should be, by its nature, less expensive than a deuterium arc system and much less expensive than ZAA, especially if electromagnetic modulation is used.

The disadvantages of the SH system compared to ZAA consist in:

1. A smaller "modulation depth" resulting in reduction of the sensitivity by 10 to 75% with an average of perhaps 40%.[81]
2. Enhancement of the pulse-cycle repetition rat t_r to 50 msec, because as long as about 40 msec are needed for the dissipation of the atomic cloud generated by the high-current pulse in the case of volatile elements, e.g., Cd. This may result in sensitivity loss in the case of short real-time signals with half-intensity widths smaller than about 200 msec obtained by furnace AAS for volatile metals. On the other hand, t_r does not influence the quality of the background correction by the SH system because the time t_{mr} needed for the measurements of the low-current (measuring) signal and the high-current (reference) signal is only 5 msec. As the atomic cloud originates partly from

thermal vaporization of volatile metals, such as Cd (see Figure 14), the number density of the self-abosrbing atoms could be reduced by cooling of the hollow-cathode. As a result, a shorter repetition time t_r could be chosen. Of course, the shortest t_r or the highest repetition frequency needed for a correct compensation of the nonspecific absorption depends on the half-intensity width $\Delta t_{1/2}$ of the transient signal $A(\lambda_o) = f(t)$. On the other hand, $\Delta t_{1/2}$ depends on the volatility of the metal, the heating rate in the atomization stage, and on the construction of the atomizer. Therefore, no general statement can be made. As a rule of thumb, the repetition time t_r should be at least ten times shorter than the half-intensity width $\Delta t_{1/2}$ of the absorption signal on the real-time display.

According to the foregoing discussions, the background correction efficiency of the SH system should be the intermediate between the direct ZAA and the inverse ZAA. Taking into account that a good background correction is much more important for the furnace AAS than for the flame AAS, the conclusion may be drawn that the inverse ZAA with a constant transversal magnetic field, generated by a permanent magnet, has the highest simplicity and practicability of all seven configurations of ZAA that have been attempted.[73] Nevertheless, the inverse AAS using electromagnetic modulation and the SH system have more flexibility. These systems can be simply changed over to the conventional mode, if a high background correction efficiency is not needed, but the best sensitivity is aimed at, e.g., for the most flame AAS measurements.

B. Continuum-Source AAS

The ratio $S_A(\Delta\lambda_m)/S_A(\lambda_o)$ of the sensitivities, measured by AAS using a continuum and a line source, respectively, is given to a first approximation by the ratio $\delta\lambda_a/\Delta\lambda_m$ of the half-intensity width of the absorption profile and the spectral band width of the monochromator (see Equation 25). As a consequence, the sensitivity of the continuum-source AAS (CS-AAS) can be "preselected" by the choice of the spectral resolution. Thus, sensitivity ratio $S_A(\Delta\lambda_m)/S_A(\lambda_o)$ should approach 1 for $\Delta\lambda_m \simeq \delta\lambda_a$. Keliher and Wohlers were the first to apply high resolution AAS using an Echelle grating monochromator.[83] They showed that it was indeed possible to obtain characteristic concentrations $c_{1\%}$ and calibration curves comparable to line-source atomic absorption. As the characteristic concentrations ($c_{1\%}$) are indirectly proportional to the corresponding sensitivities (S_A), the ratio $(c_{1\%})_C/(c_{1\%})_L$ measured by atomic absorption using a continuous (index C) and a line (index L) source, respectively, is proportional to $\Delta\lambda_m/\delta\lambda_a$. This prediction is in good agreement with the results obtained[83] with flames as atomizer: the pairs $[\Delta\lambda_m/\delta\lambda_a, (c_{1\%})_C/c_{1\%})_L]$ of [0.4, 2.5], [0.7, 0.9], [1.0, 3.1], and [0.6, 0.6] were obtained for the Al 396.1, Ca 422.7, Cu 324.7, and the Na 589.0 resonance lines.

The past, present, and future prospects of the CS-AAS were presented recently in an interesting plenary lecture,[84] which was the main source of information for the preparation of this section. Two different configurations have been developed for CS-AAS: a single element wavelength-modulated atomic absorption spectrometer using a continuum source (WM-AAC),[85] and a simultaneous multielement atomic absorption spectrometer using a continuum source (SIMMAC).[86] In both systems, a 300-W high pressure xenon arc continuum lamp is used as the primary source. This source generates about 200 nm and at a resolution of 3 pm more intense signals than commercial HCLs operated at the recommended currents.

The working principles of WM-AAC and SIMMAC will be discussed shortly. The light beam first passes the atomizer and enters an Echelle grating monochromator through an entrance slit of 50 μm width and 100 μm height and of 25 μm width and 300 μm height in the case of WM-AAC and SIMMAC, respectively. Spectraspan III monochromator and

polychromator (Spectra-Metrix, Inc., Andover, Maine) was modified by mounting a quartz refractor plate (25 × 25 × 3 mm) on an optical scanner torque motor immediately behind the entrance slit. This plate moves the image of the entrance slit rapidly back and forth across the exit slit, which has the same dimensions as the entrance slit. This movement of the beam corresponds to an apparent change of the wavelength and makes a wavelength scanning in a narrow spectral range without moving the optical grating possible. The two systems mentioned above (CS-AAC and SIMMAC) are virtually different in modulation of the movement of the refractor plate and in signal processing beyond the exit slit. The single-channel WM-AAC system utilizes analogue signal-processing electronics and the absorbances are measured on a strip-chart recorder. In the multielement (SIMMAC) system a minicomputer is used to generate the wavelength modulation waveform, measure and store intensity data on 16 active channels, and average intensities, computer intensity ratios, and absorbances. The microcomputer also determines peak heights and areas and performs analytical calibration with linear and nonlinear least-squares curve fitting techniques. It is also possible to average many passes through the modulation interval in order to enhance the signal to noise of spectral profile measurement. In both systems, a real-time display of the absorption spectrum within the modulation spectral range can be displayed on an x-y oscilloscope by connecting the phototube output to the y axis and the modulation waveform to the x axis. This display is very useful for checking the wavelength drift, excessive background absorption, or unsuspected spectral interferences.[84]

The performance characteristics of a single channel WM-AAC were studied by determination of characteristic concentrations ($c_{1\%}$) and detection limits (c_L) for 32 elements.[85] Using the appropriate air/C_2H_2- or N_2O/C_2H_2-flame as atomizer, the ratio $(c_{1\%})_C/(c_{1\%})_L$ of the characteristic concentrations measured, using the continuum and line source, respectively, was $2.69 \pm 0.91_{32}$. The number of elements is given as an index of the SD. Unfortunately, this average value cannot be compared with the corresponding theoretical estimate ($\Delta\lambda_m/\delta\lambda_a$) because no spectral band widths have been published.

The ratio of the detection limits obtained[85] with flame AAS using a continuum source and line source, respectively, was worse: 9.2 on the average of the 32 published ratios. As these ratios show a large scatter between 2 and 30, and their distribution is strongly asymmetric, the calculation of a SD would not be meaningful. The large scatter is due, at least partly, to spectral interferences caused by molecular absorption at the rotation components of molecular bands of OH, CN, etc.

Recently,[84] the detection limits could be markedly improved. An average ratio $(c_L)_C/(c_L)_L$ of 3.3 and 7.6 of the corresponding characteristic concentrations have been obtained from the 34 and 9 published ratios for flame and furnace AAS, respectively.

C. Special Applications of AAS

The application of AAS for the determination of the total concentration of elements in a great number of different samples, e.g., water and effluents, body fluids, foodstuffs, airborne particles, ceramics, alloys, etc. is well documented.[59,87-89] Therefore, only some special applications of AAS will be briefly discussed here.

A rapidly growing application field of furnace AAS may be its use in the chemical speciation of traces of elements in environmental samples, like freshwater, soil water, seawater, etc. For that purpose a chemical pretreatment is necessary in order to achieve the selectivity for the special forms of the element in question, e.g., only Se(IV) is extracted by ammoniumtetramethylenedithiocarbamate (ammoniumpyrollidinedithiocarbamate, APDC) from a mixture of Se(IV) and S(VI) present in seawater.[90] The remaining Se(IV) is reduced in the aqueous phase containing 1 *M* HCl by Ti(III) to Se (IV), which is then extracted in the form of an APDC-complex. Similar extraction behavior shows the pairs As(III,V), Sb(III,V), and Te(IV,VI). Thus, the combined procedure liquid-liquid-extraction and furnace

AAS make it possible to differentiate between different oxidation state of the elements. Furthermore, thermodynamically weak complexes can be separated from strong complexes.

Problems arising in the determination of metals, extracted into an organic phase by AAS are in general: (1) reduced reproducibility due to difficulties in injection of organic solutions, and (2) metal losses in the ashing stage of the furnace heating programs due to the high volatility of some metal chelates.

Both problems can be effectively mastered by the use of aerosol introduction into a preheated graphite tube followed by matrix modification in the tube.[91] As an example, the precision of Tl determinations was studied. Tl(III) was extracted into toluene as the Tl(III)-tetramethylenedithiocarbamate TlL_3. The organic extracts were either introduced into the preheated graphite tube in the form of aerosol using the Instrumentation Laboratory FASTAC system or were pipetted manually using micropipettes. The precisions of the sensitivities S_{Tl} measured by their RCI at the 95% confidence level were, e.g., 3.0, 3.7, and 3.7% for the solvents water, toluene, and methylisobuthylketone (MIBK) in the case of aerosol introduction. The corresponding RCI values were 3.3, 7.8, and 42% for injection by micropipettes.

In order to carry out the matrix modification in the graphite tube, first aerosol generated from 0.01 *M* H_3PO_4 was introduced into the graphite tube at 150°C for 5 sec. In order to concentrate the phosphoric acid, the tube was then purged with N_2 for 5 sec. Finally, the organic extract was nebulized and introduced into the tube. The volatile TlL_3 reacts with H_3PO_4 distributed over a large surface of the graphite tube very fast. A thermally stable product, $TlPO_4$, is obtained. As many metal chelates usually extracted are volatile, such matrix modifications may be very important in the use of the furnace AAS in chemical speciation of trace elements.

Another special application field of AAS is its use in coordination chemistry for the determination of solubility products, stability constants, and extraction constants of complexes that are practically insoluble in water, but quite easily soluble in organic solvents.[62,92] A fundamental aspect of the use of AAS in this field consists in the fact that the total concentration (molarity) $[M]_t$ of the metal in question is obtained by AAS. Therefore, the solubility $[M]_t$ must be determined in the function of the concentration (molarity) [L] of the free ligand. From the solubility curve $[M]_t = f[L]$ the solubility product K_{so} and the stability constant β_n of the neutral complex ML_n are obtained. The other possibility for investigation of sparingly soluble complexes consists in the determination of the distribution coefficient q_M ($=[M]_{to}/[M]_t$) of the metal in a two-phase system, consisting of water and an organic solvent in the function of [L] again. From the analysis of the distribution curve $q_M = f[L]$ the stability constant β_n and the distribution constant K_N of the neutral complex ML_n are obtained. The total concentrations $[M]_{to}$ and $[M]_t$ in the organic (index "o") and aqueous (no index) phase, respectively, are determined by AAS.

Last, but not least, it should be stressed that various organic materials can be determined indirectly by AAS. Recently, a first book[93] was devoted to organic analysis by AAS.

D. Summary and Future Prospects

The history of the furnace AAS was strongly influenced by two alternative furnace constructions, the L'vov furnace and the Massmann furnace. In the L'vov furnace the atomization occurs under well-defined conditions because the graphite tube is maintained at constant temperature before atomization begins. The only disadvantage of this technique is the relatively complicated sample introduction. The Massman furnace makes a very simple sample introduction possible using micropipettes or autosamplers. As the tube must be heated from room temperature to the atomization temperature, the atomization conditions are less favorable than in the L'vov furnace. The advantages of both original techniques are now combined in the L'vov platform atomization technique. Together with high performance

background correction, such as the Zeeman effect background correction and the SH background correction, furnace AAS became highly reliable. Additionally, the high sensitivity and selectivity are inherent characteristics of this powerful method. It may be concluded that the application fields of furnace AAS will be further expanded in the future. Especially, an increasing use of furnace AAS in chemical speciation of elements may be forecast.

For this application, the continuum source AAS has advantages over the conventional line source AAS: (1) an excellent background correction, (2) a greatly extended analytical range, and (3) the ability to make useful simultaneous multielement measurements. However, the disadvantages are equally clear at the present time: (1) the poorer limits in the low-UV region, and (2) the complexity and high purchase cost of a multielement system. Possibly, ICP-AES and continuum multielement AAS measurements will be carried out in the future using the same high resolution spectrometer.

ACKNOWLEDGMENT

The author wishes to thank Mrs. Margrit Roth for typing the manuscript, Mr. Josef Zihlmann for accomplishing the measurements and calculations, and Mrs. Hildegard-Szöszi Magyar for preparation of the diagrams.

REFERENCES

1. **Walsh, A.,** The application of atomic absorption spectra to chemical analysis, *Spectrochim. Acta,* 7, 108, 1955.
2. **Alkemade, C. Th. J., Hollander, Tj., Snellman, W., and Zeegers, P. J. Th.,** *Metal Vapours in Flames,* Pergamon Press, Oxford, 1982, chaps. 2, 7, 8.
3. **Rubeška, I. and Svoboda, V.,** Some causes of bending of analytical curves in atomic absorption spectroscopy, *Anal. Chim. Acta,* 32, 253, 1965.
4. **Wagenaar, H. C. and de Galan, L.,** The influence of line profiles upon analytical curves for copper and silver in atomic absorption spectroscopy, *Spectrochim. Acta,* 30B, 361, 1975.
5. **Magyar, B. and Widmer, G.,** Influence of different parameters and experimental conditions upon the initial slope of calibration curves of atomic absorption spectrometry, *Talanta,* 23, 693, 1976.
6. **Magyar, B.,** *Guide-Lines to Planning Atomic Spectrometric Analysis,* Joint edition published by Akadémiai Kiado and Elsevier Scientific, Budapest, 1982, chaps. 1, 5, 6.
7. **Magyar, B. and Aeschbach, F.,** Why not ICP at atom reservoir for AAS?, *Spectrochim. Acta,* 35B, 839, 1980.
8. **Sperling, K. R.,** The tube-in-tube technique in electrothermal atomic absorption spectrometry-III. The atomization behaviour of Zn, Pb, Cu, and Ni, *Spectrochim. Acta,* 39B, 371, 1984.
9. **Magyar, B., Wampfler, B., and Zihlmann, J.,** Comparison of sensitivity and precision between tube-in-tube technique and graphite tube technique of the atomic absorption spectrometry, *GIT Fachz. Lab.,* 28, 301, 1984.
10. **L'vov, B. V.,** *Atomic Absorption Spectrochemical Analysis,* Adam Hilger, London, 1970, chaps. 3, 5.
11. **West, T. S. and Williams, X. K.,** Atomic absorption and fluorescence spectroscopy with a carbon filament atom reservoir, *Anal. Chim. Acta,* 45, 27, 1969.
12. **Frech, W. and Cedergren, A.,** Investigations of reactions involved in flameless atomic absorption procedures. VII. A theoretical and experimental study of factors influencing the determination of silicon, *Anal. Chim. Acta,* 113, 227, 1980.
13. **Matousek, J. P.,** Removal of sample vapour in electrothermal atomization studied at constant-temperature conditions, *Spectrochim. Acta,* 39B, 205, 1984.
14. **L'vov, B. V.,** Electrothermal atomization — the way toward absolute methods of atomic absorption analysis, *Spectrochim. Acta,* 33B, 153, 1977.
15. **Chakrabarti, C. L., Hamed, H. A., Wan, C. C., Li, W. C., Bertels, P. C., Gregoire, D. C., and Lee, S.,** Capacitive discharge heating in graphite furnace atomic absorption spectrometry, *Anal. Chem.,* 52, 167, 1980.
16. **Siemer, D. D. and Frech, W.,** Improving the performance of the CRA atomizer by reducing the rate of diffusional atom loss and delaying analyte volatilization, *Spectrochim. Acta,* 39B, 261, 1984.

17. **Musil, J. and Rubeška, I.,** Mathematical model of electrothermal atomization signals based on free atom redeposition, *Analyst*, 107, 588, 1982.
18. **Torsi, G. and Tessari, G.,** Influence of heating rate on analytical response in flameless atomic absorption spectrometry, *Anal. Chem.*, 45, 1812, 1973.
19. **Guerrieri, A., Lampugnani, L., and Tessari, G.,** Electrothermal atomizer measurements for the determination of the surface coverage of lead using the graphite rod atomizer, *Spectrochim. Acta*, 39B, 193, 1984.
20. **Zhou, N. G., Frech, W., and de Galan, L.,** On the relationship between heating rate and peak height in electrothermal atomic absorption spectroscopy, *Spectrochim. Acta*, 39B, 225, 1984.
21. **Kirkbright, G. F. and Sargent, M.,** *Atomic Absorption and Fluorescence Spectroscopy*, Academic Press, London, 1974, chaps. 6, 7.
22. **Weast, R. C. and Astle, M. J.,** *CRC Handbook of Chemistry and Physics*, CRC Press, Boca Raton, Fla., 1982, 1983, p. E-64, E-334, F-185.
23. **Capitelli, M. and Ferraro, C.,** Cut-off criteria of electronic partition functions: effects on spectroscopic quantities, *Spectrochim. Acta*, 31B, 323, 1976.
24. **de Galan, L., Smith, R., and Winefordner, J. D.,** The electronic partition functions of atoms and ions between 1500 K and 7000 K, *Spectrochim. Acta*, 23B, 521, 1968.
25. **Manning, D. C. and Capacho-Delgado, L.,** Dissociation and ionization effects in atomic absorption spectrochemical analysis, *Anal. Chim. Acta*, 36, 312, 1966.
26. **Kornblum, G. R. and de Galan, L.,** Ionization interference in the acetylene nitrous oxide flame, *Spectrochim. Acta*, 28B, 139, 1973.
27. **Miller, W. J.,** Ionization in combustion processes, *Oxid. Combust. Rev.*, 3, 97, 1968.
28. **Matousek, J. P.,** Interferences in electrothermal atomic absorption spectrometry, their elimination and control, *Prog. Anal. At. Spectrosc.*, 4, 247, 1981.
29. **Sturgeon, R. E. and Chakrabarti, C. L.,** Recent advances in electrothermal atomization in graphite furnace atomic absorption spectrometry, *Prog. Anal. At. Spectrosc.*, 1, 98, 1978.
30. **Schuler, K. E. and Weber, J.,** A microwave investigation of the ionization of hydrogen-oxygen and acetylene-oxygen flames, *J. Chem. Phys.*, 22, 491, 1954.
31. **Littlejohn, D. and Ottaway, J. M.,** Mechanism of atom excitation in carbon furnace atomic-emission spectrometry, *Analyst*, 104, 208, 1979.
32. **Sturgeon, R. E., Berman, S. S., and Kashyap, S.,** Microwave attenuation determination of electron concentrations in graphite and tantalum tube electrothermal atomizers, *Anal. Chem.*, 52, 1049, 1980.
33. **Lawton, J. and Weinberg, F. J.,** *Electrical Aspects of Combustion*, Clarendon Press, Oxford, 1969, chaps. 2, 5, 6.
34. **Gaydon, A. G. and Wolfhard, H. G.,** *Flames, Their Structure, Radiation, and Temperature*, 4th ed., Chapman & Hall, London, 1979, chap. 13.
35. **Kornblum, G. R. and de Galan, L.,** Spatial distribution of the temperature and the number densities of electrons and atomic and ionic species in an inductively coupled RF argon plasma, *Spectrochim. Acta*, 32B, 71, 1977.
36. **de Galan, L. and Samaey, G. F.,** Measurement of degrees of atomization in premixed laminar flames, *Spectrochim. Acta*, 25B, 245, 1970.
37. **Willis, J. B.,** Atomization problems in atomic absorption spectroscopy-II. Determination of degree of atomization in premixed flames, *Spectrochim. Acta*, 25B, 487, 1970.
38. *CRC Handbook of Spectroscopy*, Vol. 1, Robinson, J. W., Ed., CRC Press, Boca Raton, Fla., 1974, 804, 814.
39. **Browner, R. F. and Smith, D. D.,** Direct and indirect methods for transport efficiency in atomic spectrometry: a statement, *ICP Inf. Newslett.*, 10, 532, 1984.
40. **Smith, D. D. and Browner, R. F.,** Measurement of aerosol transport efficiency in atomic spectrometry, *Anal. Chem.*, 54, 533, 1982.
41. **Magyar, B. and Zihlmann, J.,** Semiquantitative determinations by atomic absorption spectrometry without preceding ascertainment of the calibration function, in *Fortschritte in der atomspektrometrischen Spurenanalytik*, Vol. 2, Welz, B., Ed., Verlag Chemie, Weinhein, 1986, 659.
42. Nomenclature, symbols, units, and their usage in spectrochemical analysis-III. Analytical flame spectroscopy and associated non-flame procedures, *Pure Appl. Chem.*, 45, 105, 1976; *Spectrochim. Acta*, 33B, 247, 1978.
43. **Browner, R. F., Boorn, A. W., and Smith, D. D.,** Aerosol transport model for atomic spectrometry, *Anal. Chem.*, 54, 1411, 1982.
44. **Corliss, C. H. and Borman, W. R.,** *Natl. Bur. Stand.*, Monograph 53, 1962.
45. **Wiese, W. L. and Fuhr, J. R.,** *J. Phys. Chem. Ref. Data*, 4 (No. 2), 263, 1975.
46. **Slavin, W. and Carnrick, G. R.,** The possibility of standardless furnace atomic absorption spectroscopy, *Spectrochim. Acta*, 39B, 271, 1984.

47. **L'vov, B. V.,** Twenty-five years of furnace atomic absorption spectroscopy, *Spectrochim. Acta*, 39B, 149, 1984.
48. **Rann, C. S.,** Absolute analysis by atomic absorption, *Spectrochim. Acta*, 23B, 827, 1968.
49. **Long, L. G. and Winefordner, J. D.,** Limit of detection, a closer look at the IUPAC definition, *Anal. Chem.*, 55, 712A, 1983.
50. **Brownlee, K. A.,** *Statistical Theory and Methodology in Science and Engineering*, John Wiley & Sons, New York, 1965, chap. 11.
51. **Miller, J. C. and Miller, J. N.,** *Statistics for Analytical Chemistry*, Ellis Horwood, Chichester, 1984, chap. 4.
52. Nomenclature, symbols, units and their usage in spectrochemical analysis-II. Data interpretation, *Pure Appl. Chem.*, 45, 99, 1976; and *Spectrochim. Acta*, 33B, 241, 1978.
53. **Liteanu, C. and Rică, I.,** *Statistical Theory and Methodology of Trace Analysis*, Ellis Horwood, Chichester, 1980, chap. 8.
54. **Matherny, M.,** Precision of results of spectrochemical analysis by emission II. Definition of the determination limit, *Spectrosc. Lett.*, 5, 221, 1972.
55. **O'Haver, T. C.,** Analytical considerations, in *Trace Analysis. Spectroscopic Methods for Elements*, Winefordner, J. D., Ed., John Wiley & Sons, New York, 1976, chap. 2.
56. *Guide to Analytical Values for IL-Spectrometers*, 982; Atomic Absorption Methods Manual, Instrumentation Laboratory, Inc., Wilmington, Maine, 1978.
57. **Morrison, G. H. and Skogerbe, R. K.,** General aspects of trace analysis, in *Trace Analysis: Physical Methods*, Interscience, New York, 1965, chap. 1.
58. **Magyar, B., Aeschbach, F., and Vonmont, H.,** Influence of the spectral band width of the monochromator upon the sensitivity of determinations by atomic absorption spectrometry, *Fresenius Z. Anal. Chem.*, 291, 193, 1978.
59. **Welz, B.,** *Atomabsorptionsspektrometrie*, 3rd ed., Verlag Chemie, Weinheim, 1983, chap. 4.
60. **de Galan, L. and Samaey, G. F.,** Some trivial causes for the bending of analytical curves in atomic absorption spectrometry, *Spectrochim. Acta*, 24B, 679, 1969.
61. **v. Gelder, Z.,** Calculation on non-linearities of the calibration curves in atomic absorption flame spectroscopy, *Spectrochim. Acta*, 25B, 669, 1970.
62. **Magyar, B. and Vonmont, H.,** Applicability of the Zeeman effect atomic absorption in coordination chemistry and trace analysis, *Spectrochim. Acta*, 35B, 177, 1980.
63. **Kuhl, J., Markowsky, G., and Torge, R.,** Sodium analysis with a tunable dye laser, *Anal. Chem.*, 44, 375, 1972.
64. **Zander, A. T., O'Haver, T. C., and Keliher, P. N.,** Continuum source atomic absorption spectrometry with high resolution and wavelength modulation, *Anal. Chem.*, 48, 1166, 1976.
65. **Willis, J. B.,** Analysis of biological materials by atomic absorption spectroscopy, in *Methods of Biochemical Analysis*, Vol. 11, Glick, D., Ed., Interscience, New York, 1968, 1.
66. **Koirtyohann, S. R. and Pickett, E. E.,** Background corrections in long path atomic absorption spectrometry, *Anal. Chem.*, 37, 601, 1965.
67. **Ballard, A. E., Stewart, D. W., Kamm, W. O., and Zuehlke, C. W.,** Photometric mercury analysis, correction for organic substances, *Anal. Chem.*, 26, 921, 1954.
68. **Ling, C.,** Sensitive simple mercury photometer using mercury resonance lamp as a monochromatic source, *Anal. Chem.*, 39, 798, 1967.
69. **Hadeishi, T. and McLaughlin, R. D.,** Hyperfine Zeeman effect atomic absorption spectrometer for mercury, *Science*, 174, 404, 1971.
70. **Koizumi, H. and Yasuda, K.,** A novel method for atomic absorption spectroscopy based on the analyte-Zeeman effect, *Spectrochim. Acta*, 31B, 523, 1976.
71. **Smith, S. B., Jr., Schleicher, R. G., and Pfeil, D. L.,** New atomic absorption background correction technique, in *Abstracts of Papers*, Pittsburgh Conf. Exposition on Anal. Chem. and Appl. Spectrosc., Atlantic City, N.J., 1982, 442.
72. **Grassam, E., Dawson, J. B., and Ellis, D. J.,** Application of the inverse Zeeman effect to background correction in electrothermal atomic-absorption analysis, *Analyst*, 102, 804, 1977.
73. **Yasuda, K., Koizumi, H., Ohishi, K., and Noda, T.,** Zeeman effect atomic absorption, in *Progress in Analytical Atomic Spectroscopy*, Chakrabarti, C. L., Ed., Pergamon Press, Oxford, 1980, 3, 299.
74. **de Loos-Vollebregt, M. T. C. and de Galan, L.,** Theory of Zeeman atomic absorption spectrometry, *Spectrochim. Acta*, 33B, 495, 1978.
75. **Smith, S. B., Jr. and Hieftje, G. M.,** A new background-correction method for atomic absorption spectrometry, *Appl. Spectrosc.*, 37, 419, 1983.
76. **Newstead, R. A., Price, W. J., and Whiteside, P. J.,** Background correction in atomic absorption analysis, *Progress in Analytical Atomic Spectroscopy*, Chakrabarti, C. L., Ed., Pergamon Press, Oxford, 1978, 1, 267.

77. **Brown, A. A., Whiteside, P. J., and Morton, S. F. N.,** Background correction capabilities of a modern spectrophotometer for use in graphite furnace atomic absorption spectrophotometry, *Spectrochim. Acta*, 38B, 49, 1983.
78. **Stephens, R.,** Zeeman modulated atomic absorption spectroscopy, *CRC Crit. Rev. Anal. Chem.*, 9, 167, 1980.
79. **Koizumi, H.,** Correction of spectral overlap interference by Zeeman atomic absorption spectrometry, *Anal. Chem.*, 50, 1101, 1978.
80. **Sotera, J. S., Stux, R. L., and Kahn, H. L.,** Significance of spectral overlap in atomic absorption spectrometry, *Anal. Chem.*, 51, 1081, 1979.
81. **Sotera, J. J. and Kahn, H. L.,** Background correction in AAS, *Am. Lab.*, p. 100, 1982.
82. **de Galan, L. and de Loos-Vollebregt, M. T. C.,** Roll-over of analytical curves in atomic absorption spectrometry arising from background correction with pulsed hollow-cathode lamps, *Spectrochim. Acta*, 39B, 1011, 1984.
83. **Keliher, P. N. and Wohlers, C. C.,** High resolution atomic absorption spectrometry using an Echelle grating monochromator, *Anal. Chem.*, 46, 682, 1974.
84. **O'Haver, T. C.,** Continuum-source atomic-absorption spectrometry: past, present and future prospects, *Analyst*, 109, 211, 1984.
85. **Messmann, J. D., Epstein, M. S., Rains, T. C., and O'Haver, T. C.,** Performance characteristics of a continuum-source wavelength-modulated atomic absorption spectrometer, *Anal. Chem.*, 55, 1055, 1983.
86. **Harnly, J. M., O'Haver, T. C., Golden, B., and Wolf, W. R.,** Background-corrected simultaneous multi-element atomic absorption spectrometer, *Anal. Chem.*, 51, 2007, 1979.
87. **Cantle, J. E.,** *Atomic Absorption Spectrometry*, Elsevier Scientific, Amsterdam, 1982.
88. **Varma, A.,** *CRC Handbook of Atomic Absorption Analysis*, CRC Press, Boca Raton, Fla., 1984.
89. *Annual Reports on Analytical Atomic Spectroscopy*, Vol. 13, Ebdon, L. and Jackson, K. W., Eds., The Royal Society of Chemistry, London, 1985.
90. **Chung, C.-H., Iwamoto, E., Yamamoto, M., and Yamamoto, Y.,** Selective determination of arsenic (III, V), antinomy (III, V), selenium (IV, VI), and tellurium (IV, VI) by extraction and graphite atomic absorption spectrometry, *Spectrochim. Acta*, 39B, 459, 1984.
91. **Magyar, B., Wampfler, B., and Würsch, A.,** Extraction of Tl(III) from Fe(III) solutions and analysis of the organic extracts by furnace AAS, in *Fortschritte in der Atomspektrometrischen Spurenanalytik*, Vol. 1, Welz, B., Ed., Verlag Chemie, Weinheim, 1984, 659.
92. **Magyar, B. and Wechsler, P.,** Applicability of the flameless atomic absorption in the coordination chemistry-II, *Talanta*, 23, 95, 1976.
93. **Hassan, S. S. M.,** *Organic Analysis Using Atomic Absorption Spectrometry*, Ellis Horwood, Chichester, 1984.